

1 **Impacts and uncertainties of climate-induced changes in**
2 **watershed inputs on estuarine hypoxia**

3
4 **Authors:** Kyle E. Hinson¹, Marjorie A.M. Friedrichs¹, Raymond G. Najjar²; Maria Herrmann²,
5 Zihao Bian³, Gopal Bhatt^{4,5}, Pierre St-Laurent¹, Hanqin Tian⁶, Gary Shenk^{7,5}

6
7 ¹Virginia Institute of Marine Science, William & Mary, Gloucester Point, VA 23062, USA

8 ²Department of Meteorology and Atmospheric Science, The Pennsylvania State University,
9 University Park, PA 16802, USA

10 ³International Center for Climate and Global Change, Auburn University, Auburn, AL 36849,
11 USA

12 ⁴Department of Civil & Environmental Engineering, The Pennsylvania State University, State
13 College, 16801, USA

14 ⁵United States Environmental Protection Agency Chesapeake Bay Program Office, Annapolis,
15 21401, USA

16 ⁶Schiller Institute for Integrated Science and Society, Department of Earth and Environmental
17 Sciences, Boston College, Chestnut Hill, MA 02467, USA

18 ⁷United States Geological Survey, Virginia/West Virginia Water Science Center, Richmond, VA
19 23228, USA

20
21 *Correspondence to:* Kyle E. Hinson (kehinson@vims.edu; kyle.e.hinson@gmail.com)

22 **Abstract**

23
24 Multiple climate-driven stressors, including warming and increased nutrient delivery, are
25 exacerbating hypoxia in coastal marine environments. Within coastal watersheds, environmental
26 managers are particularly interested in climate impacts on terrestrial processes, which may
27 undermine the efficacy of management actions designed to reduce eutrophication and consequent
28 low-oxygen conditions in receiving coastal waters. However, substantial uncertainty
29 accompanies the application of Earth System Model (ESM) projections to a regional modeling
30 framework when quantifying future changes to estuarine hypoxia due to climate change. In this
31 study, two downscaling methods are applied to multiple ESMs and used to force two
32 independent watershed models for Chesapeake Bay, a large coastal-plain estuary of the eastern
33 United States. The projected watershed changes are then used to force a coupled 3-D
34 hydrodynamic-biogeochemical estuarine model to project climate impacts on hypoxia, with
35 particular emphasis on projection uncertainties. Results indicate that all three factors (ESM,
36 downscaling method, and watershed model) are found to contribute significantly to the
37 uncertainty associated with future hypoxia, with the choice of ESM being the largest contributor.
38 Overall, in the absence of management actions, there is a high likelihood that climate change
39 impacts on the watershed will expand low-oxygen conditions by 2050, relative to a 1990s
40 baseline period; however, the projected increase in hypoxia is quite small (4%) because only
41 climate-induced changes in watershed inputs are considered and not those on the estuary itself.
42 Results also demonstrate that the attainment of established nutrient reduction targets will reduce
43 annual hypoxia by about 50% compared to the 1990s. Given these estimates, it is virtually

44 certain that fully implemented management actions reducing excess nutrient loadings will
45 outweigh hypoxia increases driven by climate-induced changes in terrestrial runoff.

46

47 **Short Summary**

48

49 Climate impacts are essential for environmental managers to consider when implementing
50 nutrient reduction plans designed to reduce hypoxia. This work highlights relative sources of
51 uncertainty in modeling regional climate impacts on the Chesapeake Bay watershed and
52 consequent declines in Bay oxygen levels. The results demonstrate that planned water quality
53 improvement goals are capable of reducing hypoxia levels by half, offsetting climate-driven
54 impacts to terrestrial runoff.

55 1 Introduction

56

57

58 Over the past several decades, estuarine and coastal ecosystems have been subject to elevated
59 levels of hypoxia relative to the open ocean (Gilbert et al., 2010), and are anticipated to be
60 affected by multiple climate change impacts including terrestrial runoff changes (Breitburg et al.,
61 2018) and rising temperatures (Whitney, 2022). Increases in precipitation volume and intensity
62 are likely to increase discharge and associated nutrient and sediment export to coastal systems
63 (Howarth et al., 2006; Lee et al., 2016; Sinha et al., 2017). Rising atmospheric temperatures will
64 increase soil temperatures and alter evapotranspiration, soil biogeochemical cycling and plant
65 responses (Schaefer and Alber, 2007; Wolkovich et al., 2012; Ator et al., 2022), also affecting
66 riverine nutrient export to marine habitats. Further changes to agricultural practices driven by
67 these same climate impacts are also likely to contribute to altered nutrient applications and
68 subsequent soil cycling (Wagena et al., 2018). Altogether, climate impacts in the terrestrial
69 environment may further eutrophy coastal ecosystems (Najjar et al., 2010), altering the
70 phenology and biogeochemical rates of nutrient consumption and exacerbating hypoxia (Testa et
71 al., 2018).

72 Future estimates of coastal hypoxia have increased substantially over the past decade, likely
73 influenced by increased access to biogeochemical modeling tools and regional climate
74 projections needed for finer scale modeling and analyses (Fennel et al., 2019). The majority of
75 coastal hypoxia climate impact studies have focused on a select few coastal locations including
76 the Baltic Sea (Meier et al., 2011a,b; Meier et al., 2012; Neumann et al., 2012; Ryabchenko et
77 al., 2016; Saraiva et al., 2019a,b; Wählström et al., 2020; Meier et al., 2021; Meier et al., 2022),
78 Chesapeake Bay (Wang et al., 2017; Irby et al., 2018; Ni et al., 2019; Testa et al., 2021; Tian et
79 al., 2021; Cai et al., 2021), and the Gulf of Mexico (Justić et al., 1996; Justić et al., 2007; Lehrter
80 et al., 2017; Laurent et al., 2018). Other projected changes to dissolved oxygen (O₂) levels have
81 been documented in nearshore environments including the North Sea (Meire et al., 2013;
82 Wakelin et al., 2020), Arabian Sea (Lachkar et al., 2019), California Current System (Dussin et
83 al., 2019; Siedlecki et al., 2021; Pozo Buil et al., 2021), and coastal waters surrounding China
84 (Hong et al., 2020; Yau et al., 2020; Zhang et al., 2021; Zhang et al., 2022). Hypoxia projections
85 in relatively smaller estuaries have also been documented in the Elbe (Hein et al., 2018),
86 Garonne (Lajaunie-Salla et al., 2018), and Long Island Sound (Whitney and Vlahos, 2021).

87 Broadly speaking, these climate impact studies apply either a range of idealized changes to
88 conduct a sensitivity study or utilize long-term projections derived from Earth System Models
89 (ESMs) (IPCC, 2013). When directly applying such projections to study regional coastal oxygen
90 responses, dynamically or statistically downscaled estimates of atmospheric and marine variables
91 are typically used to continuously simulate climate impacts or to calculate and apply a change
92 factor (Carter et al., 1994; Anandhi et al., 2011) to a shorter historical time period. Quantifying
93 the relative uncertainties from various sources including ESM, downscaling methodology,
94 internal variability, and hydrological model is not new to the field of climate research (Hawkins
95 and Sutton, 2009; Yip et al., 2011; Northrop and Chandler, 2014) or watershed applications
96 (Bosshard et al., 2013; Vetter et al., 2017; Wang et al., 2020; Ohn et al., 2021). Questions of
97 uncertainty due to climate effects in past marine ecosystem impact studies have often been
98 addressed by selecting some combination of ESMs and/or emissions scenarios (Meier et al.,
99 2011a; Ni et al., 2019; Saraiva et al., 2019b; Meier et al., 2019; Meier et al., 2021; Pozo Buil et
100 al., 2021). Additionally, some studies have also sought to account for the importance of managed
nutrient runoff from terrestrial (Irby et al., 2018; Saraiva et al., 2019a; [Bartosova et al., 2019](#);

101 [Pihlainen et al., 2020](#)) and atmospheric (Yau et al., 2020; Meier et al., 2021) sources and their
102 impacts on oxygen levels. Despite some comprehensive efforts to identify sources of uncertainty
103 in coastal oxygen projections (Meier et al., 2019; 2021), few studies have evaluated uncertainties
104 introduced by the choice of specific downscaling method and/or terrestrial model. These factors
105 represent additional sources of variability when estimating future hypoxia and are inherent in
106 regional simulations of coastal dynamics.

107 The Chesapeake Bay, which is the largest estuary in the continental United States (Kemp et
108 al., 2005), has undergone intensive management efforts to improve water quality and oxygen
109 levels over the past three decades. These management efforts have focused on the reduction of
110 excess nitrogen, phosphorus, and sediment loadings to the Bay (USEPA, 2010), and continuous
111 adaptive monitoring efforts to evaluate progress in restoring water quality (Tango and Batiuk,
112 2016). Recent analyses of monitoring data have demonstrated improvements in water quality
113 throughout the Bay despite the trajectory of recovery being slowed by extreme weather events
114 (Zhang et al., 2018). Observed lags in water quality responses to nutrient reductions (Murphy et
115 al., 2022) are also evident in recent years (Zahran et al. 2022). Despite the difficulties in
116 assessing long-term improvements in water quality due to strong interannual variability, new
117 research has demonstrated that the Chesapeake Bay is more resilient to recent and ongoing
118 climate change impacts that have decreased oxygen levels as a result of decades of nutrient load
119 reductions (Frankel et al., 2022).

120 In recent years managers have recognized the importance of investigating whether the
121 originally established Total Maximum Daily Loads (USEPA, 2010) will need to be adjusted to
122 ensure the attainment of water quality standards for the Chesapeake Bay as the climate changes
123 (Chesapeake Bay Program, 2020; Hood et al., 2021). Increasing temperatures and precipitation
124 are anticipated to affect watershed snowpack, soil moisture levels, terrestrial nutrient cycling,
125 and associated discharge, streamflow generation, and flooding (Shenk et al., 2021b), potentially
126 altering the efficacy of nutrient reduction strategies. Increases in nutrient and carbon inputs to the
127 Bay resulting from climate change and anthropogenic stressors have already been documented
128 over the course of the past century (Pan et al., 2021; Yao et al., 2021), and are anticipated to
129 increase in the 21st century as well (Wang et al., 2017; Irby et al., 2018; Ni et al., 2019). For
130 example, Irby et al. (2018) directly tested the role of future nutrient reductions via a sensitivity
131 analysis of mid-century climate effects, and found substantial alleviation of hypoxic conditions
132 when management targets were met, despite significantly increasing water temperatures.
133 However, that study applied spatially constant changes in watershed inputs derived from a
134 specific watershed model, one downscaling technique and a median estimate of ESM
135 projections. A more robust effort to produce a range of scenarios incorporating multiple
136 watershed models, downscaling techniques and ESMs is needed to assess uncertainty estimates
137 of projected hypoxia, which can be used to guide decision-making that explicitly considers what
138 levels of environmental risk are acceptable for Chesapeake Bay stakeholders.

139 The present study applies multiple downscaled ESMs to two independently developed
140 watershed models with significantly different representation of watershed processes and spatial
141 scale; both are used to force a coupled hydrodynamic-biogeochemical estuarine model in order
142 to better constrain the relative uncertainties of future terrestrial runoff estimates on estuarine
143 hypoxia (Shenk et al., 2021a). The resulting ensemble of numerical experiments includes
144 realistic climate forcings and an extensive set of regional linked watershed-estuarine
145 deterministic model simulations. The framework established in this research assesses the relative
146 uncertainties introduced by choice of ESM, downscaling methodology, and regionally focused

147 watershed model in quantifying changes to O₂ levels in the estuary. Additionally, this
148 investigation constrains the bounds of changes to Chesapeake Bay hypoxia (defined herein as O₂
149 < 2 mg L⁻¹) with and without the effects of management actions, using an ensemble of realistic
150 watershed forcings. The study provides a roadmap for environmental managers to design climate
151 impact assessments that are better able to quantify the range of possible future levels of hypoxia,
152 which can be influenced by nutrient management actions.

154 2 Methods

156 2.1 Monitoring data

157 Monthly estimates of freshwater discharge, inorganic nitrogen, and organic nitrogen at the
158 non-tidal monitoring stations nearest the head of tide of the three largest tributaries to the
159 Chesapeake Bay (Susquehanna, Potomac, and James; Fig. 1a; Table S1) were used to evaluate
160 the performance of watershed models. Discharge and nitrogen load estimates are derived from
161 observations that are collected at United States Geological Survey (USGS) stream gages and
162 comprise part of the USGS River Input Monitoring program in the Chesapeake Bay watershed.
163 Estimates for the nitrogen species were calculated using a weighted statistical regression process
164 that accounts for the variability introduced by time, discharge, and season (Hirsch et al., 2010).

165 Main stem bay observations collected over the period 1991-2000, accessible via a data
166 repository maintained by the Chesapeake Bay Program (CBP; Olson 2012; CBP DataHub 2020),
167 were used to assess estuarine model skill (see Sect. 2.3.1). Since 1984, numerous water quality
168 data have been collected along the Bay's main stem and throughout its tributaries at semi-
169 monthly to monthly intervals as part of the Water Quality Monitoring Program. These data were
170 collected at the surface, above and below the pycnocline, and at the bottom for chemical
171 variables including nitrate and organic nitrogen, and throughout the entire water column at 1-2 m
172 intervals for O₂. Twenty CBP stations were selected for model comparison at the surface and
173 bottom (Fig. 1b, Table S2), including those most frequently sampled and those located along the
174 entirety of the Bay's main channel where hypoxia commonly occurs (Officer et al., 1984; Hagy
175 et al., 2004). Estimates of annual hypoxic volume (AHV), defined as the volume of hypoxic
176 water integrated over the year (with units of volume*time), were taken from the Bever et al.
177 (2013; 2018; 2021) interpolation of O₂ measurements at 56 CBP stations.

179 2.2 Estuarine and watershed modeling tools and evaluation

180 Model simulations are conducted with ChesROMS-ECB, a fully coupled, three-dimensional,
181 hydrodynamic and Estuarine Carbon Biogeochemistry (ECB) implementation of the Regional
182 Ocean Modeling System (ROMS ; [Shchepetkin and McWilliams 2005](#)) developed for the
183 Chesapeake Bay ([Xu et al., 2011](#)) with 20 terrain-following vertical levels and an average
184 horizontal resolution of approximately 1.8 kilometers in the estuary's mainstem (Feng et al.,
185 2015; St-Laurent et al., 2020; Frankel et al., 2022). Two parameter changes were recently made
186 to improve the representation of modeled oxygen: (1) a decrease of the maximum growth rate of
187 phytoplankton, which, following Irby et al. (2018), preserves the temperature-dependent linear
188 Q₁₀ described in Lomas et al. (2002), and (2) a decrease in the critical bottom shear stress from
189 0.010 Pa to 0.007 Pa, which increases the resuspension of organic matter and is well within the
190 range of observed shear stresses evaluated by Peterson (1999).

191 Estimates of watershed discharge, nitrogen loading, and sediment loading to drive the
192 estuarine model were obtained via two independently developed models of the Chesapeake Bay

Deleted: (RIM)

Deleted: (WQMP).

195 watershed: the Dynamic Land Ecosystem Model (DLEM; Yang et al., 2015; Yao et al., 2021)
196 and the USEPA Chesapeake Bay Program’s regulatory Phase 6 Watershed Model (Phase 6;
197 Chesapeake Bay Program, 2020). Both models were applied to generate comparable reference
198 runs over the average hydrology period of 1991-2000, chosen because it reflects the decade used
199 by the Chesapeake Bay Program to calculate Total Maximum Daily Loads (USEPA, 2010) and
200 assess water quality improvements. Outputs from both watershed models were aggregated into
201 10 major river input locations (Fig. 1). Watershed outputs were mapped to estuarine variables as
202 in Frankel et al. (2022), except that a more realistic partitioning of terrestrial organic nitrogen
203 loading into labile and refractory pools was implemented such that the percent refractory organic
204 nitrogen loading increases with discharge at high flow volumes (Appendix A).

205 Atmospheric conditions, including temperature and winds, were obtained from the ERA5
206 reanalysis dataset (C3S, 2017) as in Hinson et al. (2021). Coastal boundary conditions were
207 interpolated to match the nearest physical and nutrient observations, as in previous work (Da et
208 al., 2021). In order to isolate the impacts of climate-driven changes in watershed inputs,
209 atmospheric and coastal boundary conditions were kept the same in all model simulations under
210 realistic 1991-2000 conditions, for both reference runs (1991-2000) and all future scenarios
211 (2046-2055).

212 Watershed and estuarine model skill was evaluated by comparing results from the two
213 reference scenarios to available data (see Sect. 2.1). Nash–Sutcliffe efficiencies (Nash and
214 Sutcliffe, 1970) were used to evaluate watershed model performance of freshwater discharge and
215 nutrient loadings. Estuarine model skill was evaluated by comparing model outputs matching the
216 spatio-temporal variability of observations at 20 main stem stations over the 10-year reference
217 period. Average bias (model output minus observed value) and root-mean squared difference
218 (RMSD) of annual O₂, nitrate (NO₃), and dissolved organic nitrogen (DON) concentrations were
219 calculated at the surface and bottom. AHV estimates were calculated by summing the daily
220 volume of model cells containing low-oxygen waters (O₂ < 2 mg L⁻¹), and are expressed in units
221 of km³ d following Bever et al. (2013; 2018; 2021). Daily net primary production estimates were
222 integrated over the entire water column and averaged across the Bay and month before being
223 compared to average Bay-wide estimates from Harding et al. (2002).

225 2.3 Projected changes in atmospheric temperature and precipitation

226 Mid-21st century projected changes in atmospheric temperature and precipitation under a
227 high emissions scenario (RCP 8.5) were obtained for multiple CMIP5 ESMs that were regionally
228 downscaled via two statistical methodologies: Multivariate ~~Adapted Constructed~~ Analogs
229 (MACA; Abatzoglou and Brown, 2012; downloaded from MACAv2-METDATA) and Bias-
230 ~~Correction and~~ Spatial Disaggregation (BCSD; Wood et al., 2004; downloaded from
231 Reclamation, 2013). (Note that downscaled CMIP5 ESM output was used because downscaled
232 CMIP6 ESM output was not yet available when the research began.) Downscaled MACA and
233 BCSD projections have an average spatial resolution of approximately 0.042° and 0.125°,
234 respectively. A delta approach (Prudhomme et al., 2002; Anandhi et al., 2011) was used to
235 estimate the absolute change in atmospheric temperature and fractional change in precipitation
236 over the Chesapeake Bay watershed. In this delta approach (also commonly referred to as a
237 perturbation method or change-factor method), the difference in a given climate variable (i.e., air
238 temperature or precipitation) is calculated by first subtracting monthly downscaled ESM
239 estimates averaged over a hindcast period (in this case 1981-2010) from average monthly future
240 projections (in this case 2036-2065). The resulting mean annual cycle (with monthly resolution)

Deleted: Adaptive Corrected

Deleted: Corrected

243 in the delta (i.e., the absolute change in temperature or fractional change in precipitation) is then
244 applied to reference atmospheric forcing inputs (in this case for 1991-2000) to generate future
245 watershed scenarios (in this case for 2046-2055, hereafter referred to as mid-century) and limit
246 uncertainty introduced by interannual variability. An additional step to modify precipitation
247 intensity is also included in all climate scenarios, following the methodology outlined in Shenk
248 et al. (2021b). Thirty-year averaging periods were used to limit potential biases introduced by
249 multidecadal oscillations.

250 To reduce the computational load of applying the dozens of available ESMs to our combined
251 watershed-estuarine modeling framework for a full factorial experiment, the Katsavounidis-Kuo-
252 Zhang (KKZ; Katsavounidis et al., 1994) algorithm was applied to select a subset of five ESMs
253 from both downscaled datasets. KKZ is an objective procedure for selecting a subset of members
254 that best span the spread of the full ensemble in a multivariate space. Because changes to
255 hypoxia must be computed after a subset of ESMs are selected, the downscaled results were
256 classified in terms of changes to the two variables most likely to influence hypoxia: air
257 temperature from May–October (i.e., the historic hypoxic season in Chesapeake Bay) and
258 precipitation from November–June (corresponding to the highest set of correlation coefficients
259 when regressed against historical AHV estimates; Supplementary Material; Fig. S1). The KKZ
260 algorithm first selected an ESM nearest to the center of the cluster of models in the two-
261 parameter space, which is referred to hereafter as the Center ESM, before iteratively selecting
262 additional ESMs that were furthest from the center of the distribution and other previously
263 selected ESMs (Fig. 2, Table S3). The next four selected ESMs are referred to as Hot/Wet,
264 Cool/Wet, Hot/Dry, and Cool/Dry ESMs to denote whether they are cooler, hotter, wetter, or
265 drier, relative to the Center ESM. The specific ESMs selected based on MACA and BCSD differ
266 slightly; however, three of the five models are the same (Cool/Dry, Hot/Dry, and Cool/Wet). **The**
267 **selection process incrementally adds members to those previously selected, so that the entire**
268 **ensemble is ordered and a subset of any size can be selected. This method has proven effective at**
269 **covering the largest range of outcomes using the fewest ESMs in watersheds across the United**
270 **States in previous research (Ross and Najjar, 2019).** This ESM selection process allows for a
271 more robust comparison of the distribution of ESMs from multiple downscaled datasets as
272 opposed to individual ESM comparisons that may privilege one downscaling method over
273 others. However, because inexact matches among ESMs can impact the quantification of relative
274 uncertainty (Sect. 2.5), additional scenarios were simulated as needed for the Center and
275 Hot/Wet ESMs, which were different for the two downscaling techniques (Fig. 2, Table S3).
276 Future change in temperature and precipitation between the two downscaling methods are shown
277 for the Center ESM (Fig. 3); changes for the other four ESMs are found in the Supplementary
278 Material (Fig. S2).

280 2.4 Experiments

281 Three numerical experiments (sets of simulations) were conducted to evaluate the impacts of
282 climate scenario factors, management conditions, and the use of a subset of ESMs on future
283 AHV projections and uncertainty (Table 1). To isolate climate impacts on AHV from the
284 watershed alone, direct atmospheric and oceanic forcings to the Bay were held the same as in the
285 reference simulations (see Sect. 2.3) for all experiments. The first experiment (Multi-Factor)
286 evaluates the relative change in AHV (hereafter defined as Δ AHV) between the 1991-2000 and
287 2046-2055 time periods due to the following factors: ESM, downscaling method, and watershed
288 model (Table 1, Fig. 4). Atmospheric deltas from ten downscaled ESMs (five from MACA and

Moved down [1]: previously selected, so that the entire ensemble is ordered and a subset of any size can be selected. This method has proven effective at covering the largest range of outcomes using the fewest ESMs in watersheds across the United States in previous research (Ross and Najjar, 2019).

Deleted: The selection process incrementally adds members to the ones

Moved (insertion) [1]

297 five from BCSD) were applied directly to the two watershed models for a total of 20 simulations.
298 A separate Phase 6 climate-reference run is used to evaluate the impacts of climate alone by
299 holding land use and nutrient applications constant. This differs slightly from the Phase 6
300 reference run that simulates realistic and interannually varying nutrient inputs and terrestrial
301 conditions and is compared against observations (Sect. 2.2). Two additional simulations were
302 conducted with Phase 6 to account for the fact that the ESMs selected by the KKZ method were
303 not identical for MACA and BCSD (Table 1, Fig. 2).

304 The second experiment (Management) applied the same deltas used for Phase 6 MACA
305 scenarios in the Multi-Factor experiment, (thereby varying runoff and nutrient loading), but also
306 included the effect of changing environmental management conditions, (affecting nutrient inputs
307 to and export from the terrestrial environment), for a total of five additional simulations. These
308 Management simulations assume that reduction targets for nutrient and sediment runoff are met
309 in accordance with established management goals (USEPA, 2010). One additional scenario was
310 conducted in which management goals were imposed, and climate change was not.

311 The third experiment (All ESMs) applied all 20 MACA downscaled ESM deltas to the
312 DLEM scenarios without any changes to management conditions, thereby only modifying
313 changes in runoff and nutrient export without intentional nutrient reductions, for a total of 20
314 additional simulations. Comparing the results of the first (Multi-Factor) and third (All ESMs)
315 experiments highlights the strengths and limitations of using a subset of ESMs.

317 2.5 Climate scenario analyses

318 To analyze climate impacts on Chesapeake Bay hypoxia, changes in O₂ and AHV were
319 compared between the reference runs and the future simulations. Relative O₂ impacts introduced
320 by the three climate scenario factors (ESM, downscaling method, and watershed model) were
321 determined by applying an analysis of variance (ANOVA) approach to average ΔAHV estimates
322 for each climate scenario. This method has been previously applied to the quantification of
323 uncertainty sources in climate and hydrological applications (Hawkins and Sutton, 2009; Yip et
324 al., 2011; Bosshard et al., 2013; Ohn et al., 2021). To use this method in this study, an average
325 annual metric is first calculated for an outcome of interest (i.e., change in discharge, nitrogen
326 loading, or hypoxic volume) within the Multi-Factor experiment. Then, the relative uncertainty is
327 determined by calculating the sum of squares due to individual effects for each experimental
328 factor (ESM, downscaling method, or watershed model). Following Ohn et al. (2021), the
329 cumulative uncertainty is quantified for successive uncertainties introduced by each factor as
330 well as their interactions, removing the unexplained interaction term described in Bosshard et al.
331 (2013). The two additional ESM scenarios described previously (Table 1, Table S3) were used
332 due to the inexact matches between MACA and BCSD ESMs selected by KKZ. Despite five
333 ESMs being used in combination with only two downscaling methods and two watershed models
334 in this analysis, the approach outlined (Bosshard et al., 2013; Ohn et al., 2021) accounts for this
335 factor imbalance (five vs. two) by repeatedly subsampling combinations of two ESM scenarios
336 from the five available. An example of this methodological approach is described in Appendix B.

337 Relative frequency histograms and cumulative distributions were used to quantify the overall
338 likelihoods of increasing/decreasing ΔAHV across the entire range of future scenarios. Average
339 changes in the spatial distribution of O₂ over the typical hypoxia season (May–September) were
340 compared among all climate scenarios with no changes to management conditions. Results were
341 considered significant if at least 80% of model scenarios tested agree on the direction of O₂
342 change in the estuary, as in Tebaldi et al. (2011).

Deleted: ,

Deleted: ,

345

346 **3 Results**

347

348 **3.1 Model Skill**

349

350 **3.1.1 Watershed Models**

351

352 Modeled discharge, nitrate loading, and organic nitrogen loading from the three largest Bay
353 tributaries are comparable to observed monthly estimates derived from weighted statistical
354 regressions (see Sect. 2.1). At the most downstream USGS stations on the Susquehanna,
355 Potomac, and James Rivers, both Phase 6 and DLEM discharge estimates have higher skill
356 (Nash–Sutcliffe Efficiencies closer to 1.0) relative to nitrate and organic nitrogen loading
357 estimates (Table 2, Fig. S3). Although the overall skill of Phase 6 and DLEM is similar, Phase 6
358 generally exhibits higher model skill than DLEM in estimating monthly nitrate loading, while
359 DLEM demonstrates greater skill in simulating organic nitrogen loading.

360

361 **3.1.2 Estuarine Model**

362

363 The two reference simulations, forced with loadings from DLEM and Phase 6, demonstrate
364 substantial skill in representing key main stem estuarine biogeochemical variables, including O₂,
365 NO₃, DON, primary production, and AHV (Table 3) throughout the Bay’s mainstem. Overall, all
366 modeled variables at the surface and bottom forced by both DLEM and Phase 6 lie within 1
367 standard deviation of observations. Modeled O₂ is slightly greater than spatio–temporally paired
368 observations at the bottom, and slightly lower than observations at the surface throughout the
369 entire year (Table 3) and in the summer period of hypoxia (Fig. 5a-b), leading to a bias that is
370 relatively small compared to the standard deviations of observed O₂ concentrations across the
371 entire year (Table 3). Additionally, modeled O₂ performs similarly to or better than the results
372 included in the multi-model comparison presented in Irby et al. (2016). Modeled average annual
373 NO₃ and DON are also within the range of observations at both the surface and bottom (Table 3).
374 Whole Bay net primary production agrees well with observed estimates (Harding et al., 2002)
375 reported over a similar time period (Table 3). Finally, modeled AHV compares favorably to data-
376 derived interpolated estimates (Table 3; Fig. 5c), with increased hypoxia in wet years compared
377 to dry years. Average AHV estimates using Phase 6 and DLEM inputs are, respectively, 16%
378 and 26% greater than interpolated observations (Table 3; Fig. 5c) and approximately half the
379 model estimates lie within the estimated uncertainties (RMS % error) of the interpolation
380 methodology ($\pm 13\%$; Bever et al., 2018). Model estimates of AHV are generally slightly greater
381 when ChesROMS-ECB is forced by DLEM watershed outputs as opposed to those from Phase 6
382 (Table 3; Fig. 5c).

383

384 **3.2 Future (mid-21st century) projections of watershed discharge and nutrient loading**

385

386 Increasing temperatures and changing precipitation throughout the Bay watershed produce
387 different discharge responses for the two watershed models. On average, Phase 6 climate
388 scenarios increase watershed runoff relative to the reference run by 4–6% while DLEM climate
389 scenarios decrease average flow by 1–4% (Table 4). The annual flow changes range from -12 to
390 +15% among ESM scenarios, with wetter ESMs tending to increase annual watershed discharge

391 while drier ESM scenarios generally decrease average watershed runoff, with a lesser impact due
392 to atmospheric warming (Table 4; Fig. 6a). For both watershed models and downscaling
393 methods, the Cool/Wet ESM produces the greatest increase in annual discharge. Overall, the
394 greatest variability in changes to discharge estimates is due to ESM, as MACA and BCSD
395 scenarios increase or decrease annual discharge by comparable amounts (Table 4; Fig 6a).

396 Chesapeake Bay Phase 6 watershed model climate scenarios increase average annual total
397 nitrogen (TN) by +30% and +45% for MACA and BCSD respectively, but do not substantially
398 change DLEM TN loads (+1% and -2% for MACA and BCSD, respectively; Fig. 7). Greater
399 Phase 6 TN loadings are primarily due to extreme values in the Cool/Wet climate scenarios and
400 are driven by increases in refractory DON (Fig. 7a). While DLEM scenarios show increases in
401 the percentage of inorganic nitrogen and labile organic forms of total nitrogen loads, the
402 contribution of particulate organic nitrogen (PON) decreases, resulting in little to no increases in
403 overall TN loading (Fig. 7a). Phase 6 produces wetter climate scenarios increasing TN loading
404 more than drier scenarios (Table 4; Fig 6b), with this effect being most pronounced for the
405 Cool/Wet ESM. Phase 6 also produces the greatest percent changes in the southern rivers (James,
406 York, Rappahannock), while DLEM produces similar percent changes in all rivers (Fig. 7b).
407 Some Phase 6 climate scenarios substantially increase the average loading change in smaller
408 watersheds like the Rappahannock and York, which increase TN between 77-172% and 32-
409 430%, respectively, and are comparable to the absolute change in Susquehanna TN loading (Fig.
410 7b). In contrast with the Multi-Factor experiment results, climate scenarios that include
411 management actions substantially reduce TN loading (-28%; Fig. 7, Table 4). Like other Phase 6
412 climate scenarios that don't account for management actions, the proportion of refractory organic
413 nitrogen increases for the climate scenarios with management (+49%), but in these cases the
414 average labile inorganic and organic nitrogen loadings also substantially decrease (-40%).

415 3.3 Effects of future watershed change on estuarine O₂

416
417
418 Climate change impacts on watershed discharge and nitrogen loading substantially affect
419 estuarine hypoxia, even when, as in this study, direct climate effects on the Bay are not
420 considered. On average, the Multi-Factor climate scenarios decrease average summer bottom O₂
421 in the Bay's mainstem while also slightly increasing O₂ at the surface in some mid-Bay areas
422 (Fig. 8). In the northern part of the mainstem near the Susquehanna River outfall, model results
423 show consistent decreases in both bottom and surface summer O₂ (Fig. 8e,f). Further down the
424 main stem in the mid-Bay, surface O₂ increases in wet years, and experiences almost no change
425 in dry years (Fig. 8b,c). In the same region, bottom O₂ declines less during wet years and
426 worsen during dry years (Fig. 8e,f). Increasing O₂ levels are found in the shallow portions of the
427 major tidal tributaries (i.e., Potomac and James), but are more pronounced in wet years than dry
428 years (Fig. 8b-c,e-f). Altogether, average summer surface O₂ increases by $0.02 \pm 0.03 \text{ mg L}^{-1}$
429 (average change and standard deviation) while bottom O₂ decreases by $0.03 \pm 0.06 \text{ mg L}^{-1}$.

430 There are some clear distinctions in the overall changes to future AHV when evaluating all
431 Multi-Factor experiments. Climate effects on the watershed in DLEM increase AHV more so
432 than in Phase 6 (5.6% vs 3.1%, respectively), but the overall standard deviation of DLEM Δ AHV
433 results are greater than those for Phase 6 (Table 5). Similarly, using MACA vs. BCSD results in
434 greater changes in Δ AHV (4.8% vs. 3.9%), albeit this difference due to the choice of
435 downscaling method is less than that due to the choice of watershed model. Depending on the
436 choice of ESM, Δ AHV ranges between +0.9% (for the Cool/Dry ESM) to +8.3 % (for the

437 Cool/Wet ESM) with the Center ESM producing intermediate results (+4.4 %). When comparing
438 the impact of a particular ESM, wetter models tend to produce greater Δ AHV than drier
439 scenarios (Fig. 6c), although interannual variability is still large. When climate scenarios are
440 downscaled using different methodologies (either MACA or BCSD), average Δ AHVs have some
441 notable differences, e.g., applying the Cool/Dry model to Phase 6 produces opposite average
442 changes to hypoxia depending on downscaling method (Fig. 6c). Considering all possible
443 combinations of scenarios, ESM average annual projected AHV spans a range of 921-939 km³ d
444 for Phase 6 and 1019-1049 km³ d for DLEM, and four out of five of the climate scenarios in the
445 Multi-Factor experiment projecting increases in average AHV (Table 4).

446 When the full distribution of Multi-Factor scenarios is evaluated, the average and standard
447 deviation of these annual Δ AHV results are estimated to be 37 ± 64 km³ d ($4.4 \pm 7.4\%$; Fig 9).
448 Wetter ESMs (blues in Fig. 9a) are more likely to increase hypoxia compared to drier ESMs,
449 despite differences in downscaling method or watershed model. The likelihoods of the Cool/Dry
450 or Hot/Dry ESM increasing hypoxia are only 58% or 50%, respectively, but these chances are
451 greater than 80% for the Center, Hot/Wet, and Cool/Wet ESMs (Fig. 9a). Altogether, the Multi-
452 Factor experiment results in 72% of the runs increasing AHV when considering climate change
453 impacts on terrestrial runoff (Fig. 9b). (Note, however, that this cannot technically be considered
454 to be a statistical probability as the KKZ selection process used to generate our sample of climate
455 scenarios is neither random nor independent.)

456 The All-ESMs experiment produces similar results to those obtained when only a subset of
457 five ESMs are used. Specifically, Δ AHV increases by $6.3 \pm 3.5\%$ using only five KKZ-selected
458 ESMs and by $9.6 \pm 1.7\%$ when using all 20 ESMs (Fig. 10a,b; Model IDs further defined in
459 Table S3). The use of five KKZ-selected ESMs covers approximately 69% of the total range of
460 all 20 ESMs (Fig. 10c). Despite more than 15,000 options to choose from when selecting five out
461 of 20 ESMs, the subset selected in this work demonstrates an improved ability to outperform a
462 random selection of five ESMs (Fig. 10c) and generates a useful range of hypoxia projections.

463 The results of the Management experiment demonstrate the substantial impact of future
464 nutrient reductions on hypoxia, decreasing average AHV by $50 \pm 7\%$ relative to the 1990s
465 (Δ AHV = -438 ± 47 km³ d; Table 4; Fig. 11). Because there is a linear relationship between
466 Δ AHV computed with Phase 6 MACA scenarios including management actions (Δ AHV_{mgmt}) and
467 those without (Δ AHV = $0.56 * \Delta$ AHV<sub>mgmt} - 262; $R^2=0.59$, Fig. S5), Δ AHV_{mgmt} can be estimated
468 for any scenario by applying this linear model to the non-management scenario distribution. [In](#)
469 [effect, this linear relationship demonstrates a similar magnitude of relative nutrient export to and](#)
470 [consequent hypoxia within the estuary.](#) The result is a decrease of approximately 417 ± 67 km³ d
471 among all scenarios, within the range of the management scenario subset obtained here by
472 applying only MACA downscaled ESMs to Phase 6. As expected, hypoxia increases in the
473 Management experiment when climate impacts are also included relative to the reference
474 management scenario, specifically by 17.1 ± 34.8 km³ d or $3.8 \pm 7.8\%$ (Table 4; Fig 6c).</sub>

475 476 **3.4 Contributions to Climate Scenario Uncertainty**

477
478 Applying an ANOVA approach (Ohn et al., 2021) to watershed discharge, nutrient loadings,
479 and Δ AHV within the Multi-Factor experiment reveals that the relative uncertainties introduced
480 by the choice of ESM, downscaling method, and watershed model vary substantially (Fig. 12).
481 The choice of ESM is the dominant factor affecting changes to watershed discharge and nutrient
482 loadings (Fig. 12a-c), and comprises 59-74% of the total uncertainty. The choice of watershed

483 model is the next largest source of uncertainty, making up 17-34% of the total variance in
484 watershed changes, while the downscaling method only contributes 3-14%. Uncertainty in
485 projected organic nitrogen loadings is particularly affected by the choice of watershed model,
486 overwhelming the variability introduced by downscaling method, and strongly affecting
487 estimates of total nitrogen change. Unlike changes to watershed flow and loadings, the
488 uncertainty of projected changes to hypoxia is much more evenly distributed among the three
489 scenario factors: 40%, 25%, and 35%, for ESM, downscaling method, and watershed model
490 respectively (Fig. 12d).

491 4 Discussion

492 4.1 Uncertainty in Climate Scenario Projections

493
494
495 Projected changes in watershed discharge and nutrient delivery to the Chesapeake Bay
496 produce modest increases in estuarine hypoxia, with medium confidence (Mastrandrea et al.,
497 2010). **Hypoxic volume** has a high degree of interannual variability, and future hypoxia estimates
498 **are highly sensitive to** the choice of ESM, downscaling method, and watershed model (Fig. 6c).
499 While certain factors (particularly ESM and greenhouse gas emissions scenarios; Meier et al.,
500 2021) have previously been extensively evaluated in coastal systems with regards to **future**
501 hypoxia, the results presented here also demonstrate the importance of terrestrial forcings on
502 estuarine oxygen levels.

503
504 In this study, future changes in watershed discharge, nitrogen loadings, and estuarine hypoxia
505 are found to be highly dependent on the selection of a specific ESM (Fig. 12), comprising a
506 majority of the total uncertainty in watershed **runoff** and the greatest fraction of total uncertainty
507 for O₂ levels. When only the effect of ESM choice is considered (and downscaling and
508 hydrological model options are not; Fig. 10), the average projected change in AHV using only
509 three ESMs (often chosen to represent cool, median, and hot scenarios) has a greater standard
510 error than the selection of five in this study. Directly comparing results from the experiment that
511 compared five ESMs, two downscaling methods, and two watershed models (Multi-Factor)
512 versus that which only considered the impact of multiple ESMs (All ESMs) shows a substantial
513 overlap in the range of projected Δ AHV. In addition, multiple ESMs downscaled with a single
514 methodology and applied to one hydrological model produced meaningfully different estimates
515 of Δ AHV than a more balanced approach (Fig. 11).

516 Inter-model variability among ESMs appears to contribute most substantially to differences
517 in Bay watershed inputs, but the choice of downscaling methodology can also affect these
518 projections. The BCSD (Wood et al., 2004) and MACA (Abatzoglou and Brown, 2012)
519 downscaling methodologies used here employ different approaches to reduce historical ESM
520 biases, impacting the variability of spatio-temporal watershed hydrologic and water quality
521 responses. The ability to statistically downscale ESMs accurately depends on the spatially
522 coarser ESM's ability to simulate synoptic-scale (~1000 km) patterns and may still
523 underestimate the distributional tails of changes to temperature and precipitation. This increases
524 the importance of properly selecting a subset of ESMs (Abatzoglou and Brown, 2012).

525 Watershed model variability is caused by differences in the representation of processes that
526 affect discharge, those controlling the fate and transport of nutrients from land and in rivers, and
527 lag times of groundwater transport. The two watershed models used here project substantially
528 different results in watershed discharge and nitrogen delivery, even when the same changes to

Moved down [2]: Watershed Climate Scenario Impacts on Riverine Export and Hypoxia

The climate scenario projections evaluated in this study are in near complete agreement that the Chesapeake Bay watershed will be warmer and experience greater levels of precipitation by mid-century, yet these results are not as straightforward to interpret as they relate to changes in discharge, nutrient loads, and estuarine hypoxia. Climate impacts on extreme river flows are currently evident at global scales (Gudmundsson et al., 2021), and projected increases in precipitation that could shape such events are aligned with estimates for this region derived from observational (Yang et al., 2021) and modeling (Huang et al., 2021) studies, as well as for other regions at similar latitudes (Bevacqua et al., 2021; Madakumbura et al., 2021). However, differences exist in the spatial distribution and timing of these precipitation increases, as well as in the temperature-affected rates of evapotranspiration. As a result, these estimates produce varied projections for future freshwater discharge. These complex interactions make it difficult to directly predict future discharge from projected precipitation changes, and even more difficult to relate these to changes in nutrient loading. For example, in this study half of the climate scenarios produce increasing discharge on an annual basis, yet more than 75% of these scenarios increase total nitrogen loading. Differences in the representation of soil and riverine nitrogen processes between watershed models also results in inconsistent simulated responses of nitrogen export to similar precipitation rates. Disparate export of nitrogen species (i.e.,

Moved down [3]: Average bottom main stem O₂ levels from May–September are expected to decrease most in the southern half of the Bay (south of 38.5°N), particularly in climatologically dry years (Fig. 8).

Moved down [4]: Irby et al.

Moved down [5]: Our findings are focused on Chesapeake Bay hypoxia, but some lessons can also be drawn from other coastal ecosystems where changes in watershed discharge and nutrient loadings are also projected. In the Baltic Sea,

Deleted: 4.1

Deleted: Our analysis quantifies changes in hypoxia due to mid-century climate change impacts on watershed hydrologic and water quality responses, and provides an estimate of the relative uncertainty in estuarine hypoxi... [1]

Deleted: Again, it is important to remember that these spatially varying changes only account for the effects of climate change on watershed response in isolation, and... [2]

Deleted: (2018) suggest that increasing atmospheric temperatures are likely to uniformly decrease O₂ levels throughout the Bay's main stem, increasing temperatures at the ocean boundary during warmer months when hypo... [3]

Deleted: 4.2

Deleted: AHV

Deleted: can be modified substantially by

Deleted: outcomes

681 meteorological forcings are applied (Fig. 6). DLEM projects no change or decreases in discharge
682 for nearly all scenarios, as opposed to greater average increases in discharge for Phase 6
683 scenarios (Fig. 6a), likely driven by differences in the representation of evapotranspiration.
684 Explicit soil biogeochemical processes within DLEM increase nitrification rates in warmer
685 climate scenarios, producing higher nitrate loadings than Phase 6 despite comparable discharge
686 changes (Fig. 6b). The greater total nitrogen loadings produced by Phase 6 are largely a
687 consequence of its parameterizations for erosion and refractory nitrogen bound to sediment.
688 Increases in bioavailable nitrate loadings, unlike refractory organic nitrogen that comprises the
689 majority of DON loadings, produce greater levels of primary production and remineralization
690 within the estuary. This largely explains the discrepancy between watershed model hypoxia
691 estimates (Table 5).

692 Our findings demonstrate the importance of considering differences among these three
693 factors (ESM, downscaling, and watershed model) that may contribute to a wider range of target
694 water quality variables and living resource responses in coastal marine ecosystems like the
695 Chesapeake Bay that are highly influenced by watershed processes. Hydrological model
696 assumptions can have potentially significant impacts on estuarine hypoxia. For example, the
697 relatively high organic nitrogen loadings in Phase 6 compared to DLEM's comparatively modest
698 exports under the same future scenarios result in different levels of annual hypoxia. While
699 dramatic increases in organic nitrogen loadings within Bay tributaries are mostly limited to
700 Cool/Wet Phase 6 scenarios, there is precedent for catastrophic erosion within the Bay watershed
701 driven by extreme precipitation events (Springer et al., 2001). The relative uncertainty
702 introduced by individual factors is also not necessarily equivalent for discharge, nitrogen
703 loadings, and AHV (Fig. 12). The complex connections between terrestrial runoff and
704 biogeochemical changes in the marine environment may expand further when higher order
705 trophic-level species are considered, and even more so when direct atmospheric impacts on the
706 Bay are also included. It is unlikely that general conclusions regarding the relative impacts of
707 different factors can be drawn for a marine ecosystem when only uncertainties in watershed
708 discharge and nutrient loadings are considered. Had our results only accounted for the impacts of
709 these factors on watershed changes and not estuarine oxygen levels, the role of downscaling
710 could be incorrectly assumed to contribute negligible variability to hypoxic volume (Fig. 12). It
711 is the complex interactions of nitrogen species transformations within this estuarine model that
712 are responsible for this somewhat unexpected large contribution of downscaling method
713 uncertainty that is less prominent in watershed changes.

714 Despite the relatively small magnitude of Chesapeake Bay watershed climate impacts on
715 estuarine hypoxia compared to previous evaluations of other climate impacts, like atmospheric
716 warming over the Bay (Irby et al., 2018; Ni et al., 2019; Tian et al., 2021), the relative
717 contributions of ESM and downscaling effects to the total uncertainty are large and are also
718 likely to expand the range of outcomes for other climate sensitivity studies in this region. This
719 suggests that, when attempting to determine a likely range of ecosystem outcomes, selecting
720 additional downscaling techniques and hydrological model responses should be considered in
721 addition to the more common practice of only selecting multiple ESMs.

723 4.2 Watershed Climate Scenario Impacts on Riverine Export and Hypoxia

724
725 The climate scenario projections evaluated in this study are in near complete agreement that
726 the Chesapeake Bay watershed will be warmer and experience greater levels of precipitation by

Moved (insertion) [2]

727 mid-century, yet these results are not as straightforward to interpret as they relate to changes in
728 discharge, nutrient loads, and estuarine hypoxia. Climate impacts on extreme river flows are
729 currently evident at global scales (Gudmundsson et al., 2021), and projected increases in
730 precipitation that could shape such events are aligned with estimates for this region derived from
731 observational (Yang et al., 2021) and modeling (Huang et al., 2021) studies, as well as for other
732 regions at similar latitudes (Bevacqua et al., 2021; Madakumbura et al., 2021). However,
733 differences exist in the spatial distribution and timing of these precipitation increases, as well as
734 in the temperature-affected rates of evapotranspiration. As a result, these estimates produce
735 varied projections for future freshwater discharge. These complex interactions make it difficult
736 to directly predict future discharge from projected precipitation changes, and even more difficult
737 to relate these to changes in nutrient loading. For example, in this study half of the climate
738 scenarios produce increasing discharge on an annual basis, yet more than 75% of these scenarios
739 increase total nitrogen loading. Differences in the representation of soil and riverine nitrogen
740 processes between watershed models also results in inconsistent simulated responses of nitrogen
741 export to similar precipitation rates. Disparate export of nitrogen species (i.e., nitrate and organic
742 nitrogen) between watershed models also directly affects future nutrient load projections. These
743 hydrological model differences are evidenced by DLEM's higher NO₃ outputs that offset lower
744 organic nitrogen loadings (Fig. 7a), and are discussed further in depth in Sect. 4.2.

745 Our analysis quantifies changes in hypoxia due to mid-century climate change impacts on the
746 watershed, and provides an estimate of the relative uncertainty in these estimates. Our
747 experimental findings suggest that, in the absence of management actions, mid-century climate
748 impacts on the Chesapeake Bay watershed will increase hypoxia, specifically annual hypoxic
749 volume (AHV), by an average of $4 \pm 7\%$. This estimate is in good agreement with prior studies
750 that examined the impacts of watershed actions alone. Jrby et al. (2018) applied a sensitivity
751 approach and projected increases in AHV of 5%, while Wang et al. (2017) showed increases in
752 annual anoxic volume of 9.7%, nearly equivalent to an increase of $10 \pm 16.5\%$ found here (Table
753 6). Results from this study also project that changes to Bay O₂ levels will vary spatially. Average
754 bottom main stem O₂ levels from May–September are expected to decrease most in the southern
755 half of the Bay (south of 38.5°N), particularly in climatologically dry years (Fig. 8).

756 Importantly, the projected changes presented here only account for the effects of climate
757 change on watershed response in isolation, and do not include the additional direct impacts of the
758 atmosphere and ocean. These additional changes have been estimated in other previous studies of
759 21st century impacts relative to observed conditions (Table 6). While numerous differing metrics
760 have been reported for many of these studies, including shifting dissolved oxygen concentrations
761 and water quality regulatory criteria, this work can be compared against previous results by
762 examining changes to annual hypoxic and anoxic volumes. The majority of these studies (Table
763 6) apply idealized changes to climate forcings and generally project increases in hypoxic
764 conditions. Increases in mid-21st century annual hypoxic volume due to watershed forcings
765 (+5% and $+4.4 \pm 7.4\%$) are smaller than average impacts of increasing temperatures alone
766 (+13%), while the results of changing sea level are more mixed (Table 6). However, the
767 variability in hypoxia due to watershed changes is likely greatest among these factors and may
768 substantially modify the negative effects of warming on dissolved oxygen concentrations. Our
769 results and their uncertainties generally encompass the range of future hypoxia estimates found
770 in previous research that have studied multiple climate impacts in isolation and in various
771 combinations. Future work that accounts for the sources of uncertainty explored here by applying
772 realistic climate change projections while also standardizing a metric for model results, like

Moved (insertion) [4]

Moved (insertion) [3]

773 annual hypoxic volume, will help to narrow and better quantify definitive trends due to multiple
774 factors that influence Bay dissolved oxygen.

775 Our findings are focused on Chesapeake Bay hypoxia, but some lessons can also be drawn
776 from other coastal ecosystems where changes in watershed discharge and nutrient loadings are
777 also projected. In the Baltic Sea, Meier et al. (2011b) reported that hypoxia was very likely to
778 increase regardless of ESM or climate scenario, assuming targeted reductions in accordance with
779 the Baltic Sea Action Plan (decrease of nitrogen loads by $23 \pm 5\%$) were not met. Extensive
780 studies of projected oxygen change in the Baltic Sea have repeatedly demonstrated that climate
781 impacts are likely to increase hypoxic area (BACC II, 2015 and references therein), but more
782 recent reports (Saraiva et al., 2019a; Wählström et al., 2020; Meier et al., 2021, 2022) have
783 reaffirmed that nutrient reductions in accordance with the Baltic Sea Plan are also highly likely
784 to mitigate a substantial amount of those hypoxia increases. Repeated investigations into the
785 impact of increased discharge and higher temperatures in the Gulf of Mexico demonstrate a
786 likely expansion of hypoxic area (Justić et al. 1996; Lehrter et al., 2017; Laurent et al., 2018),
787 and additional nutrient reductions required to mitigate these impacts (Justić et al., 2003). Finally,
788 Whitney and Vlahos (2021) demonstrated a considerable erosion in oxygen gains due to nutrient
789 reductions in the presence of climate effects, reducing projected mid-century improvements by
790 14%, similar to the 9% increase in hypoxic volume reported by Irby et al. (2018) for O_2 levels $<$
791 2 mg L^{-1} . Although these studies include direct climate change impacts on coastal water bodies,
792 most support the findings here demonstrating that increases in discharge and associated nutrient
793 loadings are likely to increase Chesapeake Bay hypoxia. Overall, climate impacts on land have
794 the potential to profoundly modify biogeochemical interactions in the coastal zone and limit the
795 efficacy of nutrient reductions.

797 4.3 Hypoxia Lessened by Impacts of Management Actions

799 Projections of changes to watershed discharge and nutrient delivery can better inform
800 regional environmental managers tasked with managing interactions among nutrient reduction
801 strategies, climate change, and coastal hypoxia (Hood et al., 2021; BACC II, 2015; Fennel and
802 Laurent, 2018). The Chesapeake Bay results provided in this analysis demonstrate that the
803 management actions mandated to improve water quality (USEPA, 2010) will decrease hypoxia
804 by roughly 50%, approximately an order of magnitude more than projected increases due only to
805 watershed climate change (Fig. 11). Therefore, nutrient reduction strategies are very likely to
806 remain effective at reducing watershed nutrient loading and its contribution to eutrophication and
807 hypoxia over a range of possible ESM scenarios (Mastrandrea et al., 2010). Should all
808 management actions be implemented as outlined in the USEPA's Total Maximum Daily Load
809 (USEPA, 2010), it is very likely that future climate impacts on Bay watershed runoff will worsen
810 Bay hypoxia by a far smaller amount, relative to 1990s reference conditions. These findings are
811 consistent with those of Irby et al. (2018) who also examined the impacts of watershed climate
812 on Chesapeake Bay hypoxia for the mid-21st century. When evaluating the effects of watershed
813 climate impacts and management actions together, Irby et al. (2018) estimated an average AHV
814 increase of $12.8 \text{ km}^3 \text{ d}$, which is well within the range of $17.1 \pm 34.8 \text{ km}^3 \text{ d}$ reported here (Table
815 6). (Interestingly, the combined impact of all climate stressors, i.e. atmosphere, ocean, and
816 watershed, increased average AHV by $24.5 \text{ km}^3 \text{ d}$, which is also within the range of the results
817 reported here). Because climate change impacts are likely to increase total nitrogen loads,
818 implementing nutrient reductions that do not account for the detrimental effects of climate

Moved (insertion) [5]

Deleted: .

820 change will reduce the likelihood of attaining water quality targets. Further quantifying a range
821 of future estimates of watershed discharge and nitrogen loading using regional models is critical
822 to understanding the possibilities and limitations of mitigating negative climate impacts via
823 nutrient reductions.

824 Recent findings support the hypothesis that nutrient reductions will improve water quality
825 despite projected climate impacts in both freshwater systems (Wade et al., 2022) and other
826 coastal marine systems (Whitney and Vlahos, 2021; Saraiva et al., 2019a; [Bartosova et al., 2019](#);
827 [Wählström et al., 2020](#); [Pihlainen et al., 2020](#); Meier et al., 2021; Große et al., 2020; Jarvis et al.,
828 2022). In the Chesapeake Bay, reduced nutrient loading (Zhang et al., 2018; Murphy et al., 2022)
829 has already helped mitigate growing climate change pressures (Frankel et al., 2022), despite
830 rapidly increasing Bay temperatures over the past 30 years (Hinson et al., 2021). Like these prior
831 studies, our findings confirm that management actions will likely produce even greater benefits
832 to O₂ in coastal zones strongly affected by terrestrial runoff. While direct effects (e.g., air
833 temperature) are expected to increase hypoxia more so than watershed changes in Chesapeake
834 Bay (Irby et al., 2018, Ni et al., 2019), the comparatively greater impacts of management actions
835 reported here are also likely to substantially reduce the overall risk from a multitude of co-
836 occurring climatic stressors.

837 **4.4 Study Limitations and Future Research Directions**

840 Despite the plainly evident finding of nutrient reduction strategies improving water quality
841 and counteracting negative climate change watershed impacts, a number of important caveats
842 should temper this conclusion. First, the subset of scenarios that include management actions is
843 limited to a set of five ESMs statistically downscaled with a single methodology and applied to
844 one watershed model. As demonstrated in this work, this assumption may oversimplify the
845 complex relationship between climate forcings and watershed model simulations, especially
846 given that DLEM scenarios produce more change in nitrate and consequently more hypoxia than
847 Phase 6 scenarios. Management actions implemented in Phase 6 nutrient reduction scenarios
848 represent a multitude of possible methods to reduce point and nonpoint source pollution that are
849 assumed to be fully implemented with a high operational efficacy by mid-century, but the true
850 performance of best management practices operating under future hydroclimatic stressors
851 remains largely unresolved (Hanson et al., 2022). Additionally, the importance of legacy
852 nitrogen inputs to the Bay may grow over time (Ator and Denver, 2015; Chang et al., 2021), and
853 can only be properly accounted for via a long-term transient simulation that accounts for
854 changing groundwater conditions.

855 A key strength of the delta method applied here is its ability to remove the influence of
856 interannual variability, which is known to strongly influence hypoxia in the Chesapeake Bay
857 (Bever et al., 2013). However, the delta method is unable to account for the impacts of
858 unanticipated extreme events, or changing patterns of precipitation intensity, duration, and
859 frequency that produce dramatic responses in sediment washoff, scour, and consequent
860 watershed organic nitrogen export. Air temperature and precipitation were the only watershed
861 model input variables adjusted in this analysis, allowing for a more equivalent comparison
862 between downscaling approaches. Future representations of watershed change may also better
863 account for changes in runoff through the inclusion of factors like ESM-estimated relative
864 humidity that can help avoid possible unreasonable amplification of potential evapotranspiration
865 that would decrease tributary discharge (Milly and Dunne, 2011) and associated nutrient loads.

866 Although main stem Bay oxygen levels are the focus of this study, watershed impacts are
867 also likely to influence water quality in smaller scale tributaries. Differences in Chesapeake Bay
868 temperatures introduced by ESM and downscaling method have also been investigated by
869 Muhling et al. (2018), and contribute to biogeochemical variability via direct impacts of
870 atmospheric temperature on Bay warming. Incorporating different facets of these relative
871 uncertainties into projections of coastal change has also been demonstrated to affect ecological
872 outcomes like those surrounding fisheries (Reum et al., 2020; Bossier et al., 2021). Thus, the
873 impacts of these uncertainties are also very likely to affect socio-economic systems tied to
874 coastal resources. The analytical method applied here is well established within climatic and
875 terrestrial settings, so the relative dearth of coastal applications (excluding Meier et al., 2021)
876 may be more related to a consequence of computational demand or greater focus on uncertain
877 parameterizations of marine biogeochemical processes (Jarvis et al., 2022) that also play a large
878 role in potential future hypoxia outcomes.

880 **5 Conclusions**

881
882 Coastal ecosystems like the Chesapeake Bay that are currently and will likely continue to be
883 negatively affected by climate impacts exhibit complex responses in future scenarios,
884 demonstrating our lack of complete system understanding. While this research reaffirms the
885 importance of management actions in reducing levels of hypoxia, it also highlights the fact that
886 uncertainties in climate-impacted watershed conditions will affect estimates of Chesapeake Bay
887 O₂ levels. Additional study of uncertainty interactions within a full climate scenario (that
888 includes the impacts of changing atmospheric and oceanic conditions) will help better quantify a
889 range of hypoxia projections, among other environmental conditions within the Chesapeake Bay.
890 These results underscore the need for additional rigorous analyses of model parameterizations
891 and their contributions to model scenario uncertainty to help identify biogeochemical processes
892 that are most sensitive to climate change impacts and warrant further investigation. The
893 development of more rapid techniques to evaluate a broader range of future water quality and
894 ecological outcomes, and an inspection of their underlying assumptions, can help provide a
895 better mechanistic understanding of complex reactions to multiple climate stressors. Like
896 ongoing efforts to reduce greenhouse gas emissions and lessen the impacts of future climate
897 change globally, continuing efforts to reduce eutrophication in coastal waters will help improve
898 ecosystem resilience and the benefits derived by communities dependent on their function.
899 Indeed, nutrient reduction plans are likely to become even more essential to managers tasked
900 with preserving the health and function of rapidly evolving coastal environments and unfamiliar
901 future conditions.

902

903 **Appendix A:**

904

905

906 Original partitioning of organic nitrogen pools from the DLEM and Phase 6 watershed
907 models was based on fixed fractions previously described in Frankel et al. (2022). There, 80% of
908 the refractory organic nitrogen (rorN) loadings from Phase 6 were allocated to the small detritus
909 nitrogen (SDeN) pool and the remainder was applied to the refractory dissolved organic nitrogen
910 (rDON) pool in ChesROMS-ECB. More realistic changes to this partitioning of watershed rorN
911 loadings were implemented, which decreased the lability of organic nitrogen loads overall. A
912 specified threshold of rorN loadings was set at the 90th percentile of reference Phase 6 watershed
913 inputs to the estuarine model, and thresholds were also set for individual river levels of discharge
914 at the 50th and 90th percentiles of Phase 6 reference simulations. Below the 50th percentile of
915 discharge levels, 80% of the rorN inputs below the specified rorN threshold were allocated to
916 ChesROMS-ECB's SDeN pool, and the remainder were assigned to the rDON pool. Between the
917 50th and 90th percentiles of discharge events, 50% of the rorN load below the specified rorN
918 threshold was apportioned to ChesROMS-ECB's SDeN and rDON pools. At the uppermost
919 levels of discharge (greater than the 90th percentile), 5% of rorN was allocated to SDeN and 95%
920 was given to rDON within ChesROMS-ECB. For any partitioning of an organic nitrogen load,
921 regardless of the level of discharge, rorN loading above this cutoff was allocated to ChesROMS-
922 ECB's rDON pool. The rorN load below this threshold was allocated according to the
923 fractionations described above. Changes to Phase 6 watershed loadings were mapped to
924 equivalent DLEM watershed input variables, following the methodology of Frankel et al. (2022).

925

Table A1. Acronyms and Abbreviations

<u>AHV</u>	<u>Annual Hypoxic Volume</u>
<u>BCSD</u>	<u>Bias-Correction and Spatial Disaggregation</u>
<u>CBP</u>	<u>Chesapeake Bay Program</u>
<u>ChesROMS-ECB</u>	<u>Chesapeake Regional Ocean Modeling System – Estuarine Carbon and Biogeochemistry</u>
<u>CMIP</u>	<u>Coupled Model Intercomparison Project</u>
<u>DIN</u>	<u>Dissolved Inorganic Nitrogen</u>
<u>DLEM</u>	<u>Dynamic Land Ecosystem Model</u>
<u>DON</u>	<u>Dissolved Organic Nitrogen</u>
<u>DSC</u>	<u>Downscaling Methodology</u>
<u>ESM</u>	<u>Earth System Model</u>
<u>KKZ</u>	<u>Katsavounidis-Kuo-Zhang (Katsavounidis et al., 1994)</u>
<u>MACA</u>	<u>Multivariate Adapted Constructed Analogs</u>
<u>Phase 6</u>	<u>Phase 6 Watershed Model</u>
<u>RCP</u>	<u>Representative Concentration Pathway</u>
<u>WSM</u>	<u>Watershed Model</u>

926

927

928

929 **Appendix B:**

930
931 An example calculation of the methodology used to calculate uncertainty for a single
932 component of the total uncertainty is provided below. Average annual changes in hypoxic
933 volume (km³ d) are shown in the table below for the Multi-Factor experiment. Values of hypoxic
934 volume are rounded to the tenth decimal place in Tables 1-3, but the rounding is not carried
935 through all calculations.

936

ESM	P6 MACA	P6 BCSD	DLEM MACA	DLEM BCSD
KKZ1	-34.3	34.6	53.4	-2.0
KKZ2	-18.8	57.7	7.2	-12.5
KKZ3	24.8	23.8	139.2	71.8
KKZ4	-10.7	-32.3	88.0	8.6
KKZ5	64.7	93.7	24.3	94.3

937
938 For the first calculation, a subset of two ESMs is selected so that the number of values is
939 balanced among ESMs, downscaling methods, and watershed models. This process will be
940 repeated for each possible combination of ESMs, ten in total {(1,2), (1,3), (1,4), ..., (4, 5)}.

941

ESM	P6 MACA	P6 BCSD	DLEM MACA	DLEM BCSD
KKZ1	-34.3	34.6	53.4	-2.0
KKZ2	-18.8	57.7	7.2	-12.5

942
943 For simplicity, the above table can be rearranged to that shown below. Additionally, the format
944 of the table below and the following equations largely mirror the format of Ohn et al. (2021).

Stage 1 (E)	Stage 2 (D)	Stage 3 (W)	\bar{Y}_x
$X_{1,1}$	$X_{2,1}$	$X_{3,1}$	-34.3
		$X_{3,2}$	53.4
	$X_{2,2}$	$X_{3,1}$	34.6
		$X_{3,2}$	-2.0
$X_{1,2}$	$X_{2,1}$	$X_{3,1}$	-18.8
		$X_{3,2}$	7.2
	$X_{2,2}$	$X_{3,1}$	57.7
		$X_{3,2}$	-12.5

945
946 First, the total variance of this subset ($U_{\{1,2,3\}}^{cumul}$) is calculated, with the subscripts of each
947 individual factor (ESM=1, DSC=2, WSM=3) denoted:

948

$$U_{\{1,2,3\}}^{cumul} = \frac{1}{N} \sum_{i=1}^N (X_i - \bar{X})^2 = 1025.1$$

949 Following this, the cumulative uncertainty due to the choice of downscaling method and
950 watershed model ($U_{\{2,3\}}^{cumul}$) is calculated by selecting all values produced individual ESMs:

951 $Y_{\{1,2\}}(x_{3,1}) = \{-34.3, 34.6, -18.8, 57.7\}$
952 $Y_{\{1,2\}}(x_{3,2}) = \{53.4, -2.0, 7.2, -12.5\}$

$$U_{\{1,2\}}^{cumul} = \frac{1}{2}(U_{\{1,2\}}^{cumul}(x_{3,1}) + U_{\{1,2\}}^{cumul}(x_{3,1})) = \frac{1}{2}(1417.0 + 631.7) = 1024.3$$

Similar variance calculations are completed for the uncertainty of the first stage alone ($U_{\{1\}}^{cumul}$), where the choice of ESM is the only constant:

$$Y_{\{1\}}(x_{2,1}, x_{3,1}) = \{-34.3, -18.8\}$$

$$Y_{\{1\}}(x_{2,1}, x_{3,2}) = \{53.4, 7.2\}$$

$$Y_{\{1\}}(x_{2,2}, x_{3,1}) = \{34.6, 57.7\}$$

$$Y_{\{1\}}(x_{2,2}, x_{3,2}) = \{-2.0, -12.5\}$$

Combining these values to calculate the uncertainty of the first stage alone (ESM) yields:

$$U_{\{1\}}^{cumul} = \frac{1}{4} \sum_{i=1}^2 \sum_{j=1}^2 (Y_{\{1\}}(x_{2,i}, x_{3,j})) = \frac{1}{4}(60.1 + 533.6 + 133.4 + 52.6) \approx 188.2$$

Applying similar calculations produces the following values necessary to compute total uncertainty for all stages:

$$U_{\{1,2,3\}}^{cumul} = 1025.1$$

$$U_{\{1,2\}}^{cumul} = 1024.3$$

$$U_{\{2,3\}}^{cumul} = 1019.9$$

$$U_{\{1,3\}}^{cumul} = 947.7$$

$$U_{\{1\}}^{cumul} = 188.2$$

$$U_{\{2\}}^{cumul} = 877.7$$

$$U_{\{3\}}^{cumul} = 913.4$$

Next, the uncertainty of the first stage is calculated by subtracting the uncertainties from other stages as follows:

$$U_{\{1,2,3\},1}^{cumul} = U_{\{1,2,3\}}^{cumul} - U_{\{2,3\}}^{cumul} = 5.1$$

$$U_{\{1,2\},1}^{cumul} = U_{\{1,2\}}^{cumul} - U_{\{2\}}^{cumul} = 146.6$$

$$U_{\{1,3\},1}^{cumul} = U_{\{1,3\}}^{cumul} - U_{\{3\}}^{cumul} = 34.4$$

$$U_{\{1\},1}^{cumul} = 188.2$$

The combined value of cumulative uncertainty for the first stage (ESM) can now be calculated:

$$\frac{1}{3}(U_{\{1,2,3\},1}^{cumul} + \frac{1}{2}U_{\{1,2\},1}^{cumul} + \frac{1}{2}U_{\{1,3\},1}^{cumul} + U_{\{1\},1}^{cumul}) = \frac{1}{3}(5.1 + 73.3 + 17.2 + 188.2) = 94.6$$

Applying the same computational steps results in cumulative uncertainties for stages 2 (Downscaling Method) and 3 (Watershed Model) of 475.5 and 480.5, respectively. These values correspond to relative uncertainties for ESM, Downscaling Method, and Watershed Model of 9%, 45%, and 46%, respectively. This procedure is then repeated for all other combinations of two ESMs {(1,3), (1,4), (1,5), ..., (4, 5)}, after which the percentage values are averaged to produce the estimates reported in our results.

Formatted: Font: Bold

991 **Competing Interests:** The authors declare that they have no conflict of interest.
992

993 **Author contribution:** MF, RN, HT, and GS were responsible for project conceptualization and
994 funding acquisition. MH, ZB, and GB were responsible for data curation used in the
995 experiments. KH and MF planned the model experiments; KH, MF, and PS are responsible for
996 the methodology (model creation). KH conducted the investigation and formal analysis, and
997 created software and visualizations of results; KH wrote the original manuscript draft; MF, RN,
998 MH, ZB, GB, PS, HT, and GS reviewed and edited the manuscript.
999

1000 **Acknowledgements:** This paper is the result of research funded by the National Oceanic and
1001 Atmospheric Administration's National Centers for Coastal Ocean Science under award
1002 NA16NOS4780207 to the Virginia Institute of Marine Science. Additional funding support was
1003 provided by the VIMS Academic Studies Office. Feedback from principal investigators, team
1004 members, and the Management Transition and Advisory Group of the Chesapeake Hypoxia
1005 Analysis & Modeling Program (CHAMP) benefited this research. The authors acknowledge
1006 William & Mary Research Computing for providing computational resources and/or technical
1007 support that have contributed to the results reported within this paper
1008 (<https://www.wm.edu/it/rc>). The authors also acknowledge the World Climate Research
1009 Programme's Working Group on Coupled Modelling, which is responsible for CMIP, and we
1010 thank the climate modeling groups (listed in Table S3 of this paper) for producing and making
1011 available their model output. For CMIP, the U.S. Department of Energy's Program for Climate
1012 Model Diagnosis and Intercomparison provides coordinating support and led development of
1013 software infrastructure in partnership with the Global Organization for Earth System Science
1014 Portals. The model results used in the manuscript are permanently archived at the W&M
1015 ScholarWorks data repository associated with this article and are available for free download
1016 (<https://doi.org/xxxx>). *Finally, the authors would like to thank the anonymous reviewer and Bo
1017 Gustafsson for their helpful and insightful comments that helped improve the manuscript.*

Deleted: (MTAG)

1019 **References**

- 1020
- 1021 Abatzoglou, J. T., & Brown, T. J.: A comparison of statistical downscaling methods suited for
1022 wildfire applications, *Int. J. Climatol.*, 32, 5, 772–780, <https://doi.org/10.1002/joc.2312>,
1023 2012.
- 1024 Anandhi, A., Frei, A., Pierson, D. C., Schneiderman, E. M., Zion, M. S., Lounsbury, D., &
1025 Matonse, A. H.: Examination of change factor methodologies for climate change impact
1026 assessment, *Water Resour. Res.*, 47, 3, 1–10, <https://doi.org/10.1029/2010WR009104>, 2011.
- 1027 Ator, S.W., and Denver, J.M.: Understanding nutrients in the Chesapeake Bay watershed and
1028 implications for management and restoration—the Eastern Shore (ver. 1.2, June 2015): U.S.
1029 Geological Survey Circular 1406, 72 p., <http://dx.doi.org/10.3133/cir1406>, 2015.
- 1030 Ator, S., Schwarz, G. E., Sekellick, A. J., & Bhatt, G.: Predicting Near-Term Effects of Climate
1031 Change on Nitrogen Transport to Chesapeake Bay, *J. Am. Water Resour. Assoc.*, 58, 4, 578–
1032 596, <https://doi.org/10.1111/1752-1688.13017>, 2022.
- 1033 BACC II Author Team: Second Assessment of Climate Change for the Baltic Sea Basin, in:
1034 *Regional Climate Studies*, Springer International Publishing, Cham,
1035 <https://doi.org/10.1007/978-3-319-16006-1>, 2015.
- 1036 [Bartosova, A., Capell, R., Olesen, J. E., Jabloun, M., Refsgaard, J. C., Donnelly, C., Hyytiäinen,](#)
1037 [K., Pihlainen, S., Zandersen, M., and Arheimer, B.: Future socioeconomic conditions may](#)
1038 [have a larger impact than climate change on nutrient loads to the Baltic Sea, *Ambio*, 48,](#)
1039 [1325–1336, <https://doi.org/10.1007/s13280-019-01243-5>, 2019.](#)
- 1040 [Basenback, N., Testa, J. M., and Shen, C.: Interactions of Warming and Altered Nutrient Load](#)
1041 [Timing on the Phenology of Oxygen Dynamics in Chesapeake Bay, *J. Am. Water Resour.*](#)
1042 [*Assoc.*, 1752–1688.13101, <https://doi.org/10.1111/1752-1688.13101>, 2022.](#)
- 1043 Bevacqua, E., Shepherd, T. G., Watson, P. A. G., Sparrow, S., Wallom, D., & Mitchell, D.:
1044 Larger Spatial Footprint of Wintertime Total Precipitation Extremes in a Warmer Climate,
1045 *Geophys. Res. Lett.*, 48, 8, <https://doi.org/10.1029/2020GL091990>, 2021.
- 1046 Bever, A. J., Friedrichs, M. A. M., Friedrichs, C. T., Scully, M. E., & Lanerolle, L. W. J.:
1047 Combining observations and numerical model results to improve estimates of hypoxic
1048 volume within the Chesapeake Bay, USA, *J. Geophys. Res. Ocean.*, 118, 10, 4924–4944,
1049 <https://doi.org/10.1002/jgrc.20331>, 2013.
- 1050 Bever, A. J., Friedrichs, M. A. M., Friedrichs, C. T., & Scully, M. E.: Estimating Hypoxic
1051 Volume in the Chesapeake Bay Using Two Continuously Sampled Oxygen Profiles, *J.*
1052 *Geophys. Res. Ocean.*, 123, 9, 6392–6407, <https://doi.org/10.1029/2018JC014129>, 2018.
- 1053 Bever, A. J., Friedrichs, M. A. M., & St-Laurent, P.: Real-time environmental forecasts of the
1054 Chesapeake Bay: Model setup, improvements, and online visualization, *Environ. Model.*
1055 *Softw.*, 140, March, <https://doi.org/10.1016/j.envsoft.2021.105036>, 2021.
- 1056 Bosshard, T., Carambia, M., Goergen, K., Kotlarski, S., Krahe, P., Zappa, M., & Schär, C.:
1057 Quantifying uncertainty sources in an ensemble of hydrological climate-impact projections,
1058 *Water Resour. Res.*, 49, 3, 1523–1536, <https://doi.org/10.1029/2011WR011533>, 2013.
- 1059 Bossier, S., Nielsen, J. R., Almroth-Rosell, E., Höglund, A., Bastardie, F., Neuenfeldt, S.,
1060 Wåhlström, I., & Christensen, A.: Integrated ecosystem impacts of climate change and
1061 eutrophication on main Baltic fishery resources, *Ecol. Modell.*, 453, May,
1062 <https://doi.org/10.1016/j.ecolmodel.2021.109609>, 2021.
- 1063 Breitburg, D., Levin, L. A., Oschlies, A., Grégoire, M., Chavez, F. P., Conley, D. J., Garçon, V.,
1064 Gilbert, D., Gutiérrez, D., Isensee, K., Jacinto, G. S., Limburg, K. E., Montes, I., Naqvi, S.

1065 W. A., Pitcher, G. C., Rabalais, N. N., Roman, M. R., Rose, K. A., Seibel, B. A., ... Zhang,
1066 J.: Declining oxygen in the global ocean and coastal waters, *Science* (80-.), 359, 6371,
1067 <https://doi.org/10.1126/science.aam7240>, 2018.

1068 C3S (Copernicus Climate Change Service): “ERA5: Fifth Generation of ECMWF Atmospheric
1069 Reanalyses of the Global Climate.” Copernicus Climate Change Service Climate Data Store
1070 (CDS). <https://cds.climate.copernicus.eu/cdsapp#!/home>, 2017.

1071 Cai, X., Shen, J., Zhang, Y. J., Qin, Q., Wang, Z., & Wang, H.: Impacts of Sea-Level Rise on
1072 Hypoxia and Phytoplankton Production in Chesapeake Bay: Model Prediction and
1073 Assessment, *J. Am. Water Resour. Assoc.*, 1–18, <https://doi.org/10.1111/1752-1688.12921>,
1074 2021.

1075 Carter, T.R., Parry, M.L., Nishioka, S. and Harasawa, H., 1994. Technical Guidelines for
1076 Assessing Climate Change Impacts and Adaptations. Intergovernmental Panel on Climate
1077 Change Working Group II. University College London and Center for Global Environmental
1078 Research, Japan. 60 pp.

1079 Chang, S. Y., Zhang, Q., Byrnes, D. K., Basu, N. B., & van Meter, K. J.: Chesapeake legacies:
1080 The importance of legacy nitrogen to improving Chesapeake Bay water quality, *Environ.*
1081 *Res. Lett.*, 16, 8, <https://doi.org/10.1088/1748-9326/ac0d7b>, 2021.

1082 Chesapeake Bay Program DataHub: <http://data.chesapeakebay.net/WaterQuality>, last access: 18
1083 April 2022.

1084 Chesapeake Bay Program. Chesapeake Assessment and Scenario Tool (CAST) Version 2019.
1085 Chesapeake Bay Program Office, <https://cast.chesapeakebay.net/>, 2020.

1086 Da, F., Friedrichs, M. A. M., St-Laurent, P., Shadwick, E. H., Najjar, R. G., & Hinson, K. E.:
1087 Mechanisms Driving Decadal Changes in the Carbonate System of a Coastal Plain Estuary, *J.*
1088 *Geophys. Res. Ocean.*, 126, 6, 1–23, <https://doi.org/10.1029/2021JC017239>, 2021.

1089 Dussin, R., Curchitser, E. N., Stock, C. A., & Van Oostende, N.: Biogeochemical drivers of
1090 changing hypoxia in the California Current Ecosystem, *Deep. Res. Part II Top. Stud.*
1091 *Oceanogr.*, 169–170, May, 104590, <https://doi.org/10.1016/j.dsr2.2019.05.013>, 2019.

1092 Easton, Z., Scavia, D., Alexander, R., Band, L., Boomer, K., Kleinman, P., Martin, J., Miller, A.,
1093 Pizzuto, J., Smith, D., Welty, C., Easton, Z., Scavia, D., Alexander, R., Band, L., Boomer,
1094 K., Kleinman, P., Martin, J., & Miller, A.: Scientific and Technical Advisory Committee
1095 Chesapeake Bay Watershed Model Phase 6 Review STAC Review Report (Vol. 47, Issue
1096 September), 2017.

1097 Feng, Y., Friedrichs, M. A. M., Wilkin, J., Tian, H., Yang, Q., Hofmann, E. E., Wiggert, J. D., &
1098 Hood, R. R.: Chesapeake Bay nitrogen fluxes derived from a land- estuarine ocean
1099 biogeochemical modeling system: Model description, evaluation, and nitrogen budgets, *J.*
1100 *Geophys. Res. Biogeosciences*, 120, 1666–1695, <https://doi.org/10.1002/2017JG003800>,
1101 2015.

1102 Fennel, K., & Laurent, A.: N and P as ultimate and proximate limiting nutrients in the northern
1103 Gulf of Mexico: Implications for hypoxia reduction strategies, *Biogeosciences*, 15, 10, 3121–
1104 3131, <https://doi.org/10.5194/bg-15-3121-2018>, 2018.

1105 Fennel, K., Gehlen, M., Brasseur, P., Brown, C. W., Ciavatta, S., Cossarini, G., Crise, A.,
1106 Edwards, C. A., Ford, D., Friedrichs, M. A. M., Gregoire, M., Jones, E., Kim, H.-C.,
1107 Lamouroux, J., Murtugudde, R., Perruche, C., and the GODAE OceanView Marine
1108 Ecosystem Analysis and Prediction Task Team: Advancing Marine Biogeochemical and
1109 Ecosystem Reanalyses and Forecasts as Tools for Monitoring and Managing Ecosystem
1110 Health, *Front. Mar. Sci.*, 6, <https://doi.org/10.3389/fmars.2019.00089>, 2019.

1111 Frankel, L. T., Friedrichs, M. A. M., St-Laurent, P., Bever, A. J., Lipcius, R. N., Bhatt, G., &
 1112 Shenk, G. W.: Nitrogen reductions have decreased hypoxia in the Chesapeake Bay: Evidence
 1113 from empirical and numerical modeling, *Sci. Total Environ.*, 814,
 1114 <https://doi.org/10.1016/j.scitotenv.2021.152722>, 2022.
 1115 Gilbert, D., Rabalais, N. N., Diaz, R. J., & Zhang, J.: Evidence for greater oxygen decline rates
 1116 in the coastal ocean than in the open ocean, *Biogeosciences*, 7, 7, 2283–2296,
 1117 <https://doi.org/10.5194/bg-7-2283-2010>, 2010.
 1118 Große, F., Fennel, K., Zhang, H., & Laurent, A.: Quantifying the contributions of riverine vs.
 1119 oceanic nitrogen to hypoxia in the East China Sea, *Biogeosciences*, 17, 10, 2701–2714,
 1120 <https://doi.org/10.5194/bg-17-2701-2020>, 2020.
 1121 Gudmundsson, L., Boulange, J., Do, H. X., Gosling, S. N., Grillakis, M. G., Koutroulis, A. G.,
 1122 Leonard, M., Liu, J., Schmied, H. M., Papadimitriou, L., Pokhrel, Y., Seneviratne, S. I.,
 1123 Satoh, Y., Thiery, W., Westra, S., Zhang, X., & Zhao, F.: Globally observed trends in mean
 1124 and extreme river flow attributed to climate change, *Science*, 371, 6534, 1159–1162,
 1125 <https://doi.org/10.1126/science.aba3996>, 2021.
 1126 Hagy, J. D., Boynton, W. R., Keefe, C. W., & Wood, K. V.: Hypoxia in Chesapeake Bay, 1950–
 1127 2001: Long-term change in relation to nutrient loading and river flow, *Estuaries*, 27, 4, 634–
 1128 658, <https://doi.org/10.1007/BF02907650>, 2004.
 1129 Hanson, J., E. Bock, B. Asfaw, and Z.M. Easton.: A systematic review of Chesapeake Bay
 1130 climate change impacts and uncertainty: watershed processes, pollutant delivery and BMP
 1131 performance. CBP/TRS-330-22. Available at <https://bit.ly/BMP-CC-synth>, 2022.
 1132 Harding, L. W., Mallonee, M. E., & Perry, E. S.: Toward a predictive understanding of primary
 1133 productivity in a temperate, partially stratified estuary, *Estuar. Coast. Shelf Sci.*, 55, 3, 437–
 1134 463, <https://doi.org/10.1006/ecss.2001.0917>, 2002.
 1135 Hawkins, E., & Sutton, R.: The potential to narrow uncertainty in regional climate predictions,
 1136 *Bull. Am. Meteorol. Soc.*, 90, 8, 1095–1107, <https://doi.org/10.1175/2009BAMS2607.1>,
 1137 2009.
 1138 Hein, B., Vieregutz, C., Wyrwa, J., Kirchesch, V., & Schöl, A.: Impacts of climate change on the
 1139 water quality of the Elbe Estuary (Germany), *J. Appl. Water Eng. Res.*, 6, 1, 28–39,
 1140 <https://doi.org/10.1080/23249676.2016.1209438>, 2018.
 1141 Hinson, K. E., Friedrichs, M. A. M., St-Laurent, P., Da, F., & Najjar, R. G.: Extent and Causes of
 1142 Chesapeake Bay Warming, *J. Am. Water Resour. Assoc.*, 1–21,
 1143 <https://doi.org/10.1111/1752-1688.12916>, 2021.
 1144 Hirsch, R. M., Moyer, D. L., & Archfield, S. A.: Weighted regressions on time, discharge, and
 1145 season (WRTDS), with an application to Chesapeake Bay river inputs, *J. Am. Water Resour.*
 1146 *Assoc.*, 46, 5, 857–880, <https://doi.org/10.1111/j.1752-1688.2010.00482.x>, 2010.
 1147 Hong, B., Liu, Z., Shen, J., Wu, H., Gong, W., Xu, H., & Wang, D.: Potential physical impacts
 1148 of sea-level rise on the Pearl River Estuary, China, *J. Mar. Syst.*, 201,
 1149 <https://doi.org/10.1016/j.jmarsys.2019.103245>, 2020.
 1150 Hood, R. R., Shenk, G. W., Dixon, R. L., Smith, S. M. C., Ball, W. P., Bash, J. O., Batiuk, R.,
 1151 Boomer, K., Brady, D. C., Cerco, C., Claggett, P., de Mutsert, K., Easton, Z. M., Elmore, A.
 1152 J., Friedrichs, M. A. M., Harris, L. A., Ihde, T. F., Lacher, L., Li, L., ... Zhang, Y. J.: The
 1153 Chesapeake Bay program modeling system: Overview and recommendations for future
 1154 development, *Ecol. Modell.*, 456, July, <https://doi.org/10.1016/j.ecolmodel.2021.109635>,
 1155 2021.

1156 Howarth, R. W., Swaney, D. P., Boyer, E. W., Marino, R., Jaworski, N., & Goodale, C.: The
 1157 influence of climate on average nitrogen export from large watersheds in the Northeastern
 1158 United States, *Biogeochemistry*, 79, 1–2, 163–186, [https://doi.org/10.1007/s10533-006-](https://doi.org/10.1007/s10533-006-9010-1)
 1159 9010-1, 2006.

1160 Huang, H., Patricola, C. M., Winter, J. M., Osterberg, E. C., & Mankin, J. S.: Rise in Northeast
 1161 US extreme precipitation caused by Atlantic variability and climate change, *Weather Clim.*
 1162 *Extrem.*, 33, January, <https://doi.org/10.1016/j.wace.2021.100351>, 2021.

1163 IPCC, 2013: *Climate Change 2013: The Physical Science Basis. Contribution of Working Group*
 1164 *I to the Fifth Assessment Report of the Intergovernmental Panel on Climate Change*
 1165 [Stocker, T.F., D. Qin, G.-K. Plattner, M. Tignor, S.K. Allen, J. Boschung, A. Nauels, Y.
 1166 Xia, V. Bex and P.M. Midgley (eds.)]. Cambridge University Press, Cambridge, United
 1167 Kingdom and New York, NY, USA, 1535 pp.

1168 Irby, I. D., Friedrichs, M. A. M., Da, F., & Hinson, K. E.: The competing impacts of climate
 1169 change and nutrient reductions on dissolved oxygen in Chesapeake Bay, *Biogeosciences*, 15,
 1170 9, 2649–2668, <https://doi.org/10.5194/bg-15-2649-2018>, 2018.

1171 Irby, I. D., Friedrichs, M. A. M., Friedrichs, C. T., Bever, A. J., Hood, R. R., Lanerolle, L. W. J.,
 1172 Scully, M. E., Sellner, K., Shen, J., Testa, J., Li, M., Wang, H., Wang, P., Linker, L., & Xia,
 1173 M.: Challenges associated with modeling low-oxygen waters in Chesapeake Bay: A multiple
 1174 model comparison, *Biogeosciences*, 13, 7, 2011–2028, [https://doi.org/10.5194/bg-12-](https://doi.org/10.5194/bg-12-20361-2015)
 1175 20361-2015, 2016.

1176 Jarvis, B. M., Pauer, J. J., Melendez, W., Wan, Y., Lehrter, J. C., Lowe, L. L., & Simmons, C.
 1177 W.: Inter-model comparison of simulated Gulf of Mexico hypoxia in response to reduced
 1178 nutrient loads: Effects of phytoplankton and organic matter parameterization, *Environ.*
 1179 *Model. Softw.*, 151, 105365, <https://doi.org/10.1016/j.envsoft.2022.105365>, 2022.

1180 Justić, D., Bierman Jr, V. J., Scavia, D., & Hetland, R. D.: Forecasting Gulf’s Hypoxia : The
 1181 Next 50 Years ? Forecasting Gulf’s Hypoxia: The Next 50 Years ?, *Estuaries and Coasts*, 30,
 1182 5, 791–801, <https://doi.org/10.1007/BF02841334>, 2007.

1183 Justić, D., Rabalais, N. N., & Turner, R. E.: Effects of climate change on hypoxia in coastal
 1184 waters: A doubled CO2 scenario for the northern Gulf of Mexico, *Limnol. Oceanogr.*, 41, 5,
 1185 992–1003, <https://doi.org/10.4319/lo.1996.41.5.0992>, 1996.

1186 Justić, D., Rabalais, N. N., & Turner, R. E.: Simulated responses of the Gulf of Mexico hypoxia
 1187 to variations in climate and anthropogenic nutrient loading, *J. Mar. Syst.*, 42, 3–4, 115–126,
 1188 [https://doi.org/10.1016/S0924-7963\(03\)00070-8](https://doi.org/10.1016/S0924-7963(03)00070-8), 2003.

1189 Katsavounidis, I., Kuo, C. C. J., & Zhang, Z.: A New Initialization Technique for Generalized
 1190 Lloyd Iteration, *IEEE Signal Process. Lett.*, 1, 10, 144–146,
 1191 <https://doi.org/10.1109/97.329844>, 1994.

1192 Kemp, W. M., Boynton, W. R., Adolf, J. E., Boesch, D. F., Boicourt, W. C., Brush, G.,
 1193 Cornwell, J. C., Fisher, T. R., Glibert, P. M., Hagy, J. D., Harding, L. W., Houde, E. D.,
 1194 Kimmel, D. G., Miller, W. D., Newell, R. I. E., Roman, M. R., Smith, E. M., & Stevenson, J.
 1195 C.: Eutrophication of Chesapeake Bay: Historical trends and ecological interactions, *Mar.*
 1196 *Ecol. Prog. Ser.*, 303, 1–29, <https://doi.org/10.3354/meps303001>, 2005.

1197 Lachkar, Z., Lévy, M., & Smith, K. S.: Strong Intensification of the Arabian Sea Oxygen
 1198 Minimum Zone in Response to Arabian Gulf Warming, *Geophys. Res. Lett.*, 46, 10, 5420–
 1199 5429, <https://doi.org/10.1029/2018GL081631>, 2019.

1200 Lajaunie-Salla, K., Sottolichio, A., Schmidt, S., Litrico, X., Binet, G., & Abril, G.: Future
 1201 intensification of summer hypoxia in the tidal Garonne River (SW France) simulated by a

1202 coupled hydro sedimentary-biogeochemical model, *Environ. Sci. Pollut. Res.*, 25, 32, 31957–
1203 31970, <https://doi.org/10.1007/s11356-018-3035-6>, 2018.

1204 Laurent, A., Fennel, K., Ko, D. S., & Lehrter, J.: Climate change projected to exacerbate impacts
1205 of coastal Eutrophication in the Northern Gulf of Mexico, *J. Geophys. Res. Ocean.*, 123, 5,
1206 3408–3426, <https://doi.org/10.1002/2017JC013583>, 2018.

1207 Lee, M., Shevliakova, E., Malyshev, S., Milly, P. C. D., & Jaffé, Peter, R.: Climate variability
1208 and extremes, interacting with nitrogen storage, amplify eutrophication risk, *Geophys. Res.*
1209 *Lett.*, 43, 7520–7528, <https://doi.org/10.1002/2016GL069254>, 2016.

1210 Lehrter, J. C., Ko, D. S., Lowe, L. L., & Penta, B.: Predicted Effects of Climate Change on
1211 Northern Gulf of Mexico Hypoxia, In D. Justić, K. A. Rose, R. D. Hetland, & K. Fennel
1212 (Eds.), *Modeling Coastal Hypoxia: Numerical Simulations of Patterns, Controls and Effects*
1213 *of Dissolved Oxygen Dynamics* (pp. 173–214) Springer https://doi.org/10.1007/978-3-319-54571-4_8, 2017.

1215 Lomas, M. W., Glibert, P. M., Shiah, F. K., & Smith, E. M.: Microbial processes and
1216 temperature in Chesapeake Bay: Current relationships and potential impacts of regional
1217 warming, *Glob. Chang. Biol.*, 8, 1, 51–70, <https://doi.org/10.1046/j.1365-2486.2002.00454.x>,
1218 2002.

1219 MACAv2-METDATA: [https://data.nal.usda.gov/dataset/climate-data-rpa-2020-assessment-](https://data.nal.usda.gov/dataset/climate-data-rpa-2020-assessment-macav2-metdata-historical-modeled-1950-2005-and-future-2006-2099-projections-conterminous-united-states-124-degree-grid-scale)
1220 [macav2-metdata-historical-modeled-1950-2005-and-future-2006-2099-projections-](https://data.nal.usda.gov/dataset/climate-data-rpa-2020-assessment-macav2-metdata-historical-modeled-1950-2005-and-future-2006-2099-projections-conterminous-united-states-124-degree-grid-scale)
1221 [conterminous-united-states-124-degree-grid-scale](https://data.nal.usda.gov/dataset/climate-data-rpa-2020-assessment-macav2-metdata-historical-modeled-1950-2005-and-future-2006-2099-projections-conterminous-united-states-124-degree-grid-scale), last access: 25 April 2018.

1222 Madakumbura, G. D., Goldenson, N., & Hall, A.: Over Global Land Areas Seen in Multiple
1223 Observational Datasets, *Nat. Commun.* <http://dx.doi.org/10.1038/s41467-021-24262-x> 2021.

1224 Mastrandrea, M.D., Field, C.B., Stocker, T.F., Edenhofer O., Ebi, K.L., Frame, D.J., Held H.,
1225 Kriegler, E., Mach, K.J., Matschoss, P.R., Plattner, G.-K., Yohe, G.W., & Zwiers, F.W.:
1226 Guidance Note for Lead Authors of the IPCC Fifth Assessment Report on Consistent
1227 Treatment of Uncertainties. Intergovernmental Panel on Climate Change (IPCC). Available
1228 at <http://www.ipcc.ch>, 2010.

1229 Meier, H. E. M., Andersson, H. C., Eilola, K., Gustafsson, B. G., Kuznetsov, I., Müller-Karulis,
1230 B., Neumann, T., & Savchuk, O. P.: Hypoxia in future climates: A model ensemble study for
1231 the Baltic Sea, *Geophys. Res. Lett.*, 38, 24, 1–6, <https://doi.org/10.1029/2011GL049929>,
1232 2011a.

1233 Meier, H. E. M., Dieterich, C., & Gröger, M.: Natural variability is a large source of uncertainty
1234 in future projections of hypoxia in the Baltic Sea, *Commun. Earth Environ.*, 2, 1,
1235 <https://doi.org/10.1038/s43247-021-00115-9>, 2021.

1236 Meier, H. E. M., Dieterich, C., Gröger, M., Dutheil, C., Börgel, F., Safonova, K., Christensen, O.
1237 B., & Kjellström, E.: Oceanographic regional climate projections for the Baltic Sea until
1238 2100, *Earth Syst. Dyn.*, 13, 159–199, <https://doi.org/10.5194/esd-13-159-2022>, 2022.

1239 Meier, H. E. M., Edman, M., Eilola, K., Placke, M., Neumann, T., Andersson, H. C.,
1240 Brunnabend, S. E., Dieterich, C., Frauen, C., Friedland, R., Gröger, M., Gustafsson, B. G.,
1241 Gustafsson, E., Isaev, A., Kniebusch, M., Kuznetsov, I., Müller-Karulis, B., Naumann, M.,
1242 Omstedt, A., ... Savchuk, O. P.: Assessment of uncertainties in scenario simulations of
1243 biogeochemical cycles in the Baltic Sea, *Front. Mar. Sci.*, 6, MAR,
1244 <https://doi.org/10.3389/fmars.2019.00046>, 2019.

1245 Meier, H. E. M., Eilola, K., & Almroth, E.: Climate-related changes in marine ecosystems
1246 simulated with a 3-dimensional coupled physical-biogeochemical model of the Baltic Sea,
1247 *Clim. Res.*, 48, 1, 31–55, <https://doi.org/10.3354/cr00968>, 2011b.

1248 Meire, L., Soetaert, K. E. R., & Meysman, F. J. R.: Impact of global change on coastal oxygen
1249 dynamics and risk of hypoxia, *Biogeosciences*, 10, 4, 2633–2653, [https://doi.org/10.5194/bg-](https://doi.org/10.5194/bg-10-2633-2013)
1250 10-2633-2013, 2013.

1251 Milly, P. C. D., & Dunne, K. A.: On the hydrologic adjustment of climate-model projections:
1252 The potential pitfall of potential evapotranspiration, *Earth Interact.*, 15, 1, 1–14,
1253 <https://doi.org/10.1175/2010EI363.1>, 2011.

1254 Muhling, B. A., Gaitán, C. F., Stock, C. A., Saba, V. S., Tommasi, D., & Dixon, K. W.: Potential
1255 Salinity and Temperature Futures for the Chesapeake Bay Using a Statistical Downscaling
1256 Spatial Disaggregation Framework, *Estuaries and Coasts*, 41, 2, 349–372,
1257 <https://doi.org/10.1007/s12237-017-0280-8>, 2018.

1258 Murphy, R. R., Keisman, J., Harcum, J., Karrh, R. R., Lane, M., Perry, E. S., & Zhang, Q.:
1259 Nutrient Improvements in Chesapeake Bay: Direct Effect of Load Reductions and
1260 Implications for Coastal Management, *Environ. Sci. Technol.*, 56, 1, 260–270,
1261 <https://doi.org/10.1021/acs.est.1c05388>, 2022.

1262 Najjar, R. G., Pyke, C. R., Adams, M. B., Breitburg, D., Hershner, C., Kemp, M., Howarth, R.,
1263 Mulholland, M. R., Paolisso, M., Secor, D., Sellner, K., Wardrop, D., & Wood, R.: Potential
1264 climate-change impacts on the Chesapeake Bay, *Estuar. Coast. Shelf Sci.*, 86, 1, 1–20,
1265 <https://doi.org/10.1016/j.ecss.2009.09.026>, 2010.

1266 Nash, J. E., & Sutcliffe, J. V.: River Flow Forecasting through Conceptual Models Part I - A
1267 Discussion of Principles*, *J. Hydrol.*, 10, 282–290, 1970.

1268 Neumann, T., Eilola, K., Gustafsson, B., Müller-Karulis, B., Kuznetsov, I., Meier, H. E. M., &
1269 Savchuk, O. P.: Extremes of temperature, oxygen and blooms in the baltic sea in a changing
1270 climate, *Ambio*, 41, 6, 574–585, <https://doi.org/10.1007/s13280-012-0321-2>, 2012.

1271 Ni, W., Li, M., Ross, A. C., & Najjar, R. G.: Large Projected Decline in Dissolved Oxygen in a
1272 Eutrophic Estuary Due to Climate Change, *J. Geophys. Res. Ocean.*, 124, 11, 8271–8289,
1273 <https://doi.org/10.1029/2019JC015274>, 2019.

1274 Northrop, P. J., & Chandler, R. E.: Quantifying sources of uncertainty in projections of future
1275 climate, *J. Clim.*, 27, 23, 8793–8808, <https://doi.org/10.1175/JCLI-D-14-00265.1>, 2014.

1276 Officer, C. B., Biggs, R. B., Taft, J. L., Cronin, L. E., Tyler, M. A., & Boynton, W. R.:
1277 Chesapeake Bay anoxia: Origin, development, and significance, *Science*, 223, 4631, 22–27,
1278 <https://doi.org/10.1126/science.223.4631.22>, 1984.

1279 Ohn, I., Kim, S., Seo, S. B., Kim, Y. O., & Kim, Y.: Model-wise uncertainty decomposition in
1280 multi-model ensemble hydrological projections, *Stoch. Environ. Res. Risk Assess.*, 35, 12,
1281 2549–2565, <https://doi.org/10.1007/s00477-021-02039-4>, 2021.

1282 Olson, M.: Guide to Using Chesapeake Bay Program Water Quality Monitoring Data, edited by
1283 M. Mallonee and M.E. Ley. Annapolis, MD: Chesapeake Bay Program, 2012.

1284 Pan, S., Bian, Z., Tian, H., Yao, Y., Najjar, R. G., Friedrichs, M. A. M., Hofmann, E. E., Xu, R.,
1285 & Zhang, B.: Impacts of Multiple Environmental Changes on Long-Term Nitrogen Loading
1286 From the Chesapeake Bay Watershed, *J. Geophys. Res. Biogeosciences*, 126, 5,
1287 <https://doi.org/10.1029/2020JG005826>, 2021.

1288 Peterson, E. L.: Benthic shear stress and sediment condition, *Aquac. Eng.*, 21, 2, 85–111,
1289 [https://doi.org/10.1016/S0144-8609\(99\)00025-4](https://doi.org/10.1016/S0144-8609(99)00025-4), 1999.

1290 [Pihlainen, S., Zandersen, M., Hyytiäinen, K., Andersen, H. E., Bartosova, A., Gustafsson, B.,](#)
1291 [Jabloun, M., McCrackin, M., Meier, H. E. M., Olesen, J. E., Sarajva, S., Swaney, D., and](#)
1292 [Thodsen, H.: Impacts of changing society and climate on nutrient loading to the Baltic Sea,](#)
1293 [Sci. Tot. Env., 731, 138935, https://doi.org/10.1016/j.scitotenv.2020.138935, 2020.](#)

1294 Pozo Buil, M., Jacox, M. G., Fiechter, J., Alexander, M. A., Bograd, S. J., Curchitser, E. N.,
1295 Edwards, C. A., Rykaczewski, R. R., & Stock, C. A.: A Dynamically Downscaled Ensemble
1296 of Future Projections for the California Current System, *Front. Mar. Sci.*, 8, April, 1–18,
1297 <https://doi.org/10.3389/fmars.2021.612874>, 2021.

1298 Prudhomme, C., Reynard, N., & Crooks, S.: Downscaling of global climate models for flood
1299 frequency analysis: Where are we now?, *Hydrol. Process.*, 16, 1137–1150,
1300 <https://doi.org/10.1002/hyp.1054>, 2002.

1301 Reum, J. C. P., Blanchard, J. L., Holsman, K. K., Aydin, K., Hollowed, A. B., Hermann, A. J.,
1302 Cheng, W., Faig, A., Haynie, A. C., & Punt, A. E.: Ensemble Projections of Future Climate
1303 Change Impacts on the Eastern Bering Sea Food Web Using a Multispecies Size Spectrum
1304 Model, *Front. Mar. Sci.*, 7, March, 1–17, <https://doi.org/10.3389/fmars.2020.00124>, 2020.

1305 Ross, A. C., & Najjar, R. G.: Evaluation of methods for selecting climate models to simulate
1306 future hydrological change, *Clim. Change*, 157, 3–4, 407–428,
1307 <https://doi.org/10.1007/s10584-019-02512-8>, 2019.

1308 Ryabchenko, V. A., Karlin, L. N., Isaev, A. V., Vankevich, R. E., Eremina, T. R., Molchanov,
1309 M. S., & Savchuk, O. P.: Model estimates of the eutrophication of the Baltic Sea in the
1310 contemporary and future climate, *Oceanology*, 56, 1, 36–45,
1311 <https://doi.org/10.1134/S0001437016010161>, 2016.

1312 Saraiva, S., Markus Meier, H. E., Andersson, H., Höglund, A., Dieterich, C., Gröger, M.,
1313 Hordoir, R., & Eilola, K.: Baltic Sea ecosystem response to various nutrient load scenarios in
1314 present and future climates, *Clim. Dyn.*, 52, 5–6, 3369–3387, <https://doi.org/10.1007/s00382-018-4330-0>, 2019a.

1315 Saraiva, S., Markus Meier, H. E., Andersson, H., Höglund, A., Dieterich, C., Gröger, M.,
1316 Hordoir, R., & Eilola, K.: Uncertainties in projections of the Baltic Sea ecosystem driven by
1317 an ensemble of global climate models, *Front. Earth Sci.*, 6, January, 1–18,
1318 <https://doi.org/10.3389/feart.2018.00244>, 2019b.

1319 Schaefer, S. C., & Alber, M.: Temperature controls a latitudinal gradient in the proportion of
1320 watershed nitrogen exported to coastal ecosystems, *Biogeochemistry*, 85, 3, 333–346,
1321 <https://doi.org/10.1007/s10533-007-9144-9>, 2007.

1322 <https://doi.org/10.1016/j.ocemod.2004.08.002>, 2005.

1323 [Shchepetkin, A. F. and McWilliams, J. C.: The Regional Oceanic Modeling System \(ROMS\): A](https://doi.org/10.1016/j.ocemod.2004.08.002)
1324 [Split-Explicit, Free-Surface, Topography-Following-Coordinate Oceanic Model. *Ocean*](https://doi.org/10.1016/j.ocemod.2004.08.002)
1325 [Modelling](https://doi.org/10.1016/j.ocemod.2004.08.002), 9, 347–404, <https://doi.org/10.1016/j.ocemod.2004.08.002>, 2005.

1326 Shenk, G., M. Bennett, D. Boesch, L. Currey, M. Friedrichs, M. Herrmann, R. Hood, T. Johnson,
1327 L. Linker, A. Miller, and D. Montali. 2021a. Chesapeake Bay Program Climate Change
1328 Modeling 2.0 Workshop. STAC Publication Number 21-003, Edgewater, MD. 35 pp.

1329 Shenk, G. W., Bhatt, G., Tian, R., Cerco, C.F., Bertani, I., Linker, L.C., 2021b. Modeling
1330 Climate Change Effects on Chesapeake Water Quality Standards and Development of 2025
1331 Planning Targets to Address Climate Change. CBPO Publication Number 328-21, Annapolis,
1332 MD. 145 pp.

1333 Siedlecki, S. A., Pilcher, D., Howard, E. M., Deutsch, C., MacCready, P., Norton, E. L., Frenzel,
1334 H., Newton, J., Feely, R. A., Alin, S. R., & Klingler, T.: Coastal processes modify projections
1335 of some climate-driven stressors in the California Current System, *Biogeosciences*, 18, 9,
1336 2871–2890, <https://doi.org/10.5194/bg-18-2871-2021>, 2021.

1337 Sinha, E., Michalak, A. M., & Balaji, V.: Eutrophication will increase during the 21st century as
1338 a result of precipitation changes, *Science*, 357, 6349, 1–5,
1339 <https://doi.org/10.1126/science.aan2409>, 2017.

1340 Springer, G. S., Dowdy, H. S., & Eaton, L. S.: Sediment budgets for two mountainous basins
1341 affected by a catastrophic storm: Blue ridge mountains, Virginia, *Geomorphology*, 37, 1–2,
1342 135–148, [https://doi.org/10.1016/S0169-555X\(00\)00066-0](https://doi.org/10.1016/S0169-555X(00)00066-0), 2001.

1343 St-Laurent, P., Friedrichs, M. A. M., Najjar, R. G., Shadwick, E. H., Tian, H., & Yao, Y.:
1344 Relative impacts of global changes and regional watershed changes on the inorganic carbon
1345 balance of the Chesapeake Bay, *Biogeosciences*, 17, 14, 3779–3796,
1346 <https://doi.org/10.5194/bg-17-3779-2020>, 2020.

1347 Tango, P. J., & Batiuk, R. A.: Chesapeake Bay recovery and factors affecting trends: Long-term
1348 monitoring, indicators, and insights, *Reg. Stu. in Mar. Sci.*, 4, 12-20,
1349 <https://doi.org/10.1016/j.rsma.2015.11.010>, 2016.

1350 Tebaldi, C., Arblaster, J. M., & Knutti, R.: Mapping model agreement on future climate
1351 projections, *Geophys. Res. Lett.*, 38, 23, 1–5, <https://doi.org/10.1029/2011GL049863>, 2011.

1352 Testa, J. M., Basenback, N., Shen, C., Cole, K., Moore, A., Hodgkins, C., & Brady, D. C.:
1353 Modeling Impacts of Nutrient Loading, Warming, and Boundary Exchanges on Hypoxia and
1354 Metabolism in a Shallow Estuarine Ecosystem, *J. Am. Water Resour. Assoc.*, 1–22,
1355 <https://doi.org/10.1111/1752-1688.12912>, 2021.

1356 Testa, J. M., Murphy, R. R., Brady, D. C., & Kemp, W. M.: Nutrient-and climate-induced shifts
1357 in the phenology of linked biogeochemical cycles in a temperate estuary, *Front. Mar. Sci.*, 5,
1358 114, <https://doi.org/10.3389/fmars.2018.00114>, 2018.

1359 Tian, R., Cerco, C. F., Bhatt, G., Linker, L. C., & Shenk, G. W.: Mechanisms Controlling
1360 Climate Warming Impact on the Occurrence of Hypoxia in Chesapeake Bay, *J. Am. Water
1361 Resour. Assoc.*, 1–21, <https://doi.org/10.1111/1752-1688.12907>, 2021.

1362 USEPA (U.S. Environmental Protection Agency): Chesapeake Bay Total Maximum Daily Load
1363 for Nitrogen, Phosphorus and Sediment. Annapolis, MD: U.S. Environmental Protection
1364 Agency Chesapeake Bay Program Office. [http://www.epa.gov/
1365 reg3wapd/tmdl/ChesapeakeBay/tmdlexec.html](http://www.epa.gov/reg3wapd/tmdl/ChesapeakeBay/tmdlexec.html), 2010.

1366 Vetter, T., Reinhardt, J., Flörke, M., van Griensven, A., Hattermann, F., Huang, S., Koch, H.,
1367 Pechlivanidis, I. G., Plötner, S., Seidou, O., Su, B., Vervoort, R. W., & Krysanova, V.:
1368 Evaluation of sources of uncertainty in projected hydrological changes under climate change
1369 in 12 large-scale river basins, *Clim. Change*, 141, 3, 419–433,
1370 <https://doi.org/10.1007/s10584-016-1794-y>, 2017.

1371 Wade, A. J., Skeffington, R. A., Couture, R.-M., Erlandsson Lampa, M., Groot, S., Halliday, S.
1372 J., Harezlak, V., Hejzlar, J., Jackson-Blake, L. A., Lepistö, A., Papastergiadou, E., Riera, J.
1373 L., Rankinen, K., Shahgedanova, M., Trolle, D., Whitehead, P. G., Psaltopoulos, D., &
1374 Skuras, D.: Land Use Change to Reduce Freshwater Nitrogen and Phosphorus will Be
1375 Effective Even with Projected Climate Change, *Water*, 14, 5, 829,
1376 <https://doi.org/10.3390/w14050829>, 2022.

1377 Wagena, M. B., Collick, A. S., Ross, A. C., Najjar, R. G., Rau, B., Sommerlot, A. R., Fuka, D.
1378 R., Kleinman, P. J. A., & Easton, Z. M.: Impact of climate change and climate anomalies on
1379 hydrologic and biogeochemical processes in an agricultural catchment of the Chesapeake
1380 Bay watershed, USA, *Sci. Total Environ.*, 637–638, 1443–1454,
1381 <https://doi.org/10.1016/j.scitotenv.2018.05.116>, 2018.

1382 Wåhlström, I., Höglund, A., Almroth-Rosell, E., MacKenzie, B. R., Gröger, M., Eilola, K.,
1383 Plikshs, M., & Andersson, H. C.: Combined climate change and nutrient load impacts on
1384 future habitats and eutrophication indicators in a eutrophic coastal sea, *Limnol. Oceanogr.*,
1385 1–18, <https://doi.org/10.1002/lno.11446>, 2020.

1386 Wakelin, S. L., Artioli, Y., Holt, J. T., Butenschön, M., & Blackford, J.: Controls on near-bed
1387 oxygen concentration on the Northwest European Continental Shelf under a potential future
1388 climate scenario, *Prog. Oceanogr.*, 93, 2020.

1389 Wang, H. M., Chen, J., Xu, C. Y., Zhang, J., & Chen, H.: A Framework to Quantify the
1390 Uncertainty Contribution of GCMs Over Multiple Sources in Hydrological Impacts of
1391 Climate Change, *Earth's Futur.*, 8, 8, <https://doi.org/10.1029/2020EF001602>, 2020.

1392 Wang, P., Linker, L., Wang, H., Bhatt, G., Yactayo, G., Hinson, K.E., & Tian, R.: Assessing
1393 water quality of the Chesapeake Bay by the impact of sea level rise and warming, *IOP Conf. Ser. Earth Environ. Sci.*, 82, 1, <https://doi.org/10.1088/1755-1315/82/1/012001>, 2017.

1395 Whitney, M. M., & Vlahos, P.: Reducing Hypoxia in an Urban Estuary despite Climate
1396 Warming, *Environ. Sci. Technol.*, 55, 2, 941–951, <https://doi.org/10.1021/acs.est.0c03964>,
1397 2021.

1398 Whitney, M.M.: Observed and projected global warming pressure on coastal hypoxia,
1399 *Biogeosciences*, 19, 4479–4497, <https://doi.org/10.5194/bg-19-4479-2022>, 2022.

1400 Wolkovich, E. M., Cook, B. I., Allen, J. M., Crimmins, T. M., Betancourt, J. L., Travers, S. E.,
1401 Pau, S., Regetz, J., Davies, T. J., Kraft, N. J. B., Ault, T. R., Bolmgren, K., Mazer, S. J.,
1402 McCabe, G. J., McGill, B. J., Parmesan, C., Salamin, N., Schwartz, M. D., & Cleland, E. E.:
1403 Warming experiments underpredict plant phenological responses to climate change, *Nature*,
1404 485, 7399, 494–497, <https://doi.org/10.1038/nature11014>, 2012.

1405 Wood, A. W., Leung, L. R., Sridhar, V., & Lettenmaier, D. P.: Hydrologic implications of
1406 dynamical and statistical approaches to downscaling climate model outputs, *Clim. Change*,
1407 62, 1–3, 189–216, <https://doi.org/10.1023/B:CLIM.0000013685.99609.9e>, 2004.

1408 [Xu, J., Long, W., Wiggert, J. D., Lanerolle, L. W. J., Brown, C. W., Murtugudde, R., and Hood, R. R.: Climate Forcing and Salinity Variability in Chesapeake Bay, USA, *Estuaries and Coasts*, 35, 237–261, <https://doi.org/10.1007/s12237-011-9423-5>, 2011.](https://doi.org/10.1007/s12237-011-9423-5)

1409

1410

1411 Yang, Q., Tian, H., Friedrichs, M. A. M., Liu, M., Li, X., & Yang, J.: Hydrological responses to
1412 climate and land-use changes along the north american east coast: A 110-Year historical
1413 reconstruction, *J. Am. Water Resour. Assoc.*, 51, 1, 47–67,
1414 <https://doi.org/10.1111/jawr.12232>, 2015.

1415 Yang, X., Wang, X., Cai, Z., & Cao, W.: Detecting spatiotemporal variations of maximum
1416 rainfall intensities at various time intervals across Virginia in the past half century, *Atmos.*
1417 *Res.*, 255, <https://doi.org/10.1016/j.atmosres.2021.105534>, 2021.

1418 Yao, Y., Tian, H., Pan, S., Najjar, R. G., Friedrichs, M. A. M., Bian, Z., Li, H. Y., & Hofmann,
1419 E. E.: Riverine Carbon Cycling Over the Past Century in the Mid-Atlantic Region of the
1420 United States, *J. Geophys. Res. Biogeosciences*, 126, 5, 1–21,
1421 <https://doi.org/10.1029/2020JG005968>, 2021.

1422 Yau, Y. Y., Baker, D. M., & Thibodeau, B.: Quantifying the Impact of Anthropogenic
1423 Atmospheric Nitrogen Deposition on the Generation of Hypoxia under Future Emission
1424 Scenarios in Chinese Coastal Waters, *Environ. Sci. Technol.*, 54, 7, 3920–3928,
1425 <https://doi.org/10.1021/acs.est.0c00706>, 2020.

1426 Yip, S., Ferro, C. A. T., Stephenson, D. B., & Hawkins, E.: A Simple, coherent framework for
1427 partitioning uncertainty in climate predictions, *J. Clim.*, 24, 17, 4634–4643,
1428 <https://doi.org/10.1175/2011JCLI4085.1>, 2011.

1429 Zahran, A. R., Zhang, Q., Tango, P., & Smith, E. P.: A water quality barometer for Chesapeake
1430 Bay: Assessing spatial and temporal patterns using long-term monitoring data, *Ecol. Indic.*,
1431 140, April, 109022, <https://doi.org/10.1016/j.ecolind.2022.109022>, 2022.

1432 Zhang, Q., Murphy, R. R., Tian, R., Forsyth, M. K., Trentacoste, E. M., Keisman, J., & Tango, P.
1433 J.: Chesapeake Bay's water quality condition has been recovering: Insights from a
1434 multimetric indicator assessment of thirty years of tidal monitoring data, *Sci. Total Environ.*,
1435 637–638, 1617–1625, <https://doi.org/10.1016/j.scitotenv.2018.05.025>, 2018.
1436 Zhang, W., Dunne, J. P., Wu, H., & Zhou, F.: Regional projection of climate warming effects on
1437 coastal seas in east China, *Environ. Res. Lett.*, 17, 7, 074006, [https://doi.org/10.1088/1748-](https://doi.org/10.1088/1748-9326/ac7344)
1438 [9326/ac7344](https://doi.org/10.1088/1748-9326/ac7344), 2022.
1439 Zhang, W., Moriarty, J. M., Wu, H., & Feng, Y.: Response of bottom hypoxia off the Changjiang
1440 River Estuary to multiple factors: A numerical study, *Ocean Model.*, 159, May 2020,
1441 <https://doi.org/10.1016/j.ocemod.2021.101751>, 2021.
1442

1443 **Tables and Figures**

1444

1445 **Table 1.** Experiments conducted to quantify future changes in Annual Hypoxic Volume (AHV).

1446

Experiment Name	Number of ESMs	Number of downscaling techniques	Number of watershed models	Number of simulations
Multi-Factor	5 ^a	2 (MACA and BCSD)	2 (DLEM and Phase 6)	20 ^b
Management	5 ^a	1 (MACA)	1 (Phase 6)	5 ^c
All-ESMs	20	1 (MACA)	1 (DLEM)	20

1447

1448

1449

1450

1451

^aCorresponding to the KKK-selected subset of five ESMs: Center, Cool/Dry, Hot/Wet, Cool/Wet, and Hot/Dry for both MACA and BCSD downscaled model outputs.

^bAdditional scenarios were simulated for the Multi-Factor experiment as needed (for the Center and Hot/Wet ESMs) to accurately partition uncertainty in model outcomes.

^cAn additional scenario simulated the effects of future management conditions without climate change impacts.

1452 **Table 2:** Nash-Sutcliffe efficiencies of the DLEM and Phase 6 Watershed Models at the most
 1453 downstream stations of three major rivers, for monthly estimates of discharge and nutrient
 1454 loading over the period 1991-2000. Nash-Sutcliffe efficiencies equal to one are indicative of
 1455 perfect model skill and negative values indicate that error variance exceeds the observed
 1456 variance.

Major River	Freshwater Discharge		Nitrate Loading		Organic Nitrogen Loading	
	DLEM	Phase 6	DLEM	Phase 6	DLEM	Phase 6
Susquehanna	0.74	0.88	0.60	0.78	0.37	0.12
Potomac	0.59	0.90	0.32	0.87	0.34	-0.69
James	0.59	0.92	-1.05	0.42	0.51	0.72

1457

1458 **Table 3:** Model skill metrics over the reference period (1991-2000)

Variable	Depth	Watershed model	ChesROMS-ECB estimate	Observed estimate ^a	Bias	RMSD
O ₂ [mg L ⁻¹]	Surface	DLEM	7.9 ± 2.3	9.3 ± 2.0	-1.4	2.2
		Phase 6	8.0 ± 2.3		-1.4	2.2
	Bottom	DLEM	6.1 ± 3.5	5.7 ± 3.5	0.4	1.7
		Phase 6	6.2 ± 3.4		0.5	1.6
NO ₃ [mmol N m ³]	Surface	DLEM	0.32 ± 0.36	0.23 ± 0.33	0.09	0.23
		Phase 6	0.30 ± 0.37		0.06	0.22
	Bottom	DLEM	0.27 ± 0.33	0.14 ± 0.24	0.13	0.25
		Phase 6	0.25 ± 0.33		0.11	0.23
DON [mmol N m ³]	Surface	DLEM	0.27 ± 0.05	0.28 ± 0.08	-0.00	0.08
		Phase 6	0.32 ± 0.08		0.05	0.12
	Bottom	DLEM	0.27 ± 0.05	0.26 ± 0.08	0.00	0.08
		Phase 6	0.31 ± 0.08		0.04	0.11
Primary Production [mg C m ⁻² d ⁻¹]	Water	DLEM	1146 ± 154 ^b	957 ± 287	189	N/A
	Column	Phase 6	1133 ± 129		176	
AHV [km ³ d]	Water	DLEM	987 ± 254	785 ± 201	202	250
	Column	Phase 6	906 ± 199		121	212

1459 ^aObserved estimates and standard deviations for O₂, NO₃, and DON are from [Water Quality Monitoring Program data](#) at 20 main
1460 stem stations. Observed estimate and standard error for primary production are derived from Harding et al. (2002), averaged over
1461 Feb-Nov for the years 1982-1998. Observed estimate and standard deviation for AHV is derived by applying a weighted-distance
1462 interpolation model to observed O₂ at a limited number of stations (Bever et al., 2013).
1463

^bModeled primary production is computed only over Feb-Nov for comparison with the observed estimate.

Deleted: the WQMP

1465 **Table 4:** Annual average and standard deviations of reference (1991-2000) and climate scenario
 1466 (2046-2055) watershed loadings and estuarine hypoxia.

Watershed Freshwater Discharge [km ³ y ⁻¹]					
Watershed Model	DLEM		Phase 6		Phase 6 with Management
1990s	84 ± 26		72 ± 21		74 ± 21
2050s Downscaling	MACA	BCSD	MACA	BCSD	MACA
Center	87 ± 28	74 ± 24	78 ± 21	80 ± 22	79 ± 21
Cool/Dry	76 ± 24	75 ± 24	67 ± 19	77 ± 22	68 ± 19
Hot/Wet	84 ± 29	86 ± 29	79 ± 22	77 ± 21	80 ± 22
Hot/Dry	77 ± 25	74 ± 23	70 ± 20	68 ± 20	72 ± 20
Cool/Wet	93 ± 29	95 ± 30	83 ± 22	80 ± 22	84 ± 22
ESM Average	84 ± 27	81 ± 26	75 ± 21	76 ± 21	77 ± 21
Watershed Nitrogen Loading [10 ⁹ gN y ⁻¹]					
Watershed Model	DLEM		Phase 6		Phase 6 with Management
1990s	151 ± 49		147 ± 46		87 ± 28
2050s Downscaling	MACA	BCSD	MACA	BCSD	MACA
Center	159 ± 46	138 ± 41	177 ± 63	192 ± 75	103 ± 36
Cool/Dry	137 ± 39	132 ± 38	133 ± 36	166 ± 53	78 ± 23
Hot/Wet	157 ± 48	153 ± 45	183 ± 66	184 ± 68	105 ± 37
Hot/Dry	149 ± 45	138 ± 41	146 ± 42	140 ± 40	86 ± 26
Cool/Wet	159 ± 43	181 ± 62	301 ± 186	352 ± 244	156 ± 85
ESM Average	152 ± 43	148 ± 48	188 ± 110	207 ± 139	105 ± 53
Annual Hypoxic Volume [km ³ d]					
Watershed Model	DLEM		Phase 6		Phase 6 with Management
1990s	987 ± 254		904 ± 171		449 ± 144
2050s Downscaling	MACA	BCSD	MACA	BCSD	MACA
Center	1072 ± 233	985 ± 250	926 ± 152	938 ± 152	470 ± 131
Cool/Dry	994 ± 252	975 ± 257	885 ± 177	961 ± 170	429 ± 148
Hot/Wet	1094 ± 247	1059 ± 249	931 ± 156	928 ± 171	480 ± 131
Hot/Dry	1075 ± 263	996 ± 259	893 ± 164	871 ± 165	442 ± 141
Cool/Wet	1011 ± 204	1081 ± 238	969 ± 170	997 ± 203	507 ± 138
ESM Average	1049 ± 234	1019 ± 244	921 ± 160	939 ± 171	466 ± 135

1467

1468 **Table 5:** Average \pm standard error in Δ AHV (%) holding scenario effects (ESM, Downscaling
 1469 Method, Watershed Model) constant.

Scenario Factor	Effect	Δ AHV ₁₄₇₀ %
ESM	Center	4.4 \pm 5.4
	Cool/Dry	0.9 \pm 4.3
	Hot/Wet	6.7 \pm 6.2
	Hot/Dry	1.4 \pm 3.6
	Cool/Wet	8.3 \pm 6.5
Downscaling	MACA	4.8 \pm 6.0
	BCSD	3.9 \pm 5.9
Watershed Model	DLEM	5.6 \pm 7.5
	Phase 6	3.1 \pm 3.8

Deleted: -----Page Break-----

Table 6: A summary comparison of simulated mid-21st century climate change impacts on Chesapeake Bay hypoxia relative to observed conditions.

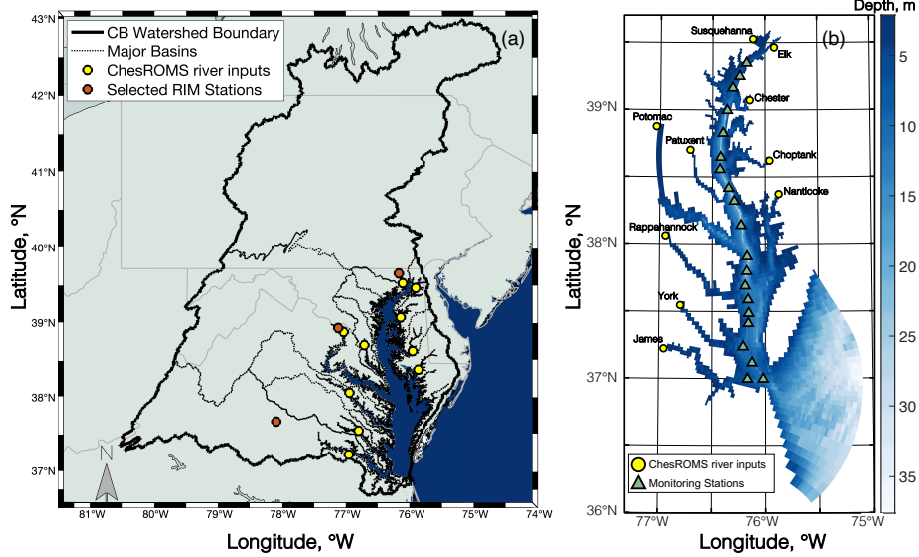
<u>Published Research</u>	<u>Climate Change Factors</u>	<u>Future Oxygen Change</u>
Watershed Changes		
<u>Wang et al., 2017</u>	Increased watershed nitrogen loadings by +5 to +10%	No AHV estimate provided Increase in AAV*: +9.7 to +18.7%
<u>Irby et al., 2018</u>	Changed watershed discharge by -2% to +17% (varying by month); assumed nutrient reductions	Increase in AHV: +5%
<u>Hinson et al., 2023** (this paper)</u>	Changed watershed loadings according to two watershed models, two downscaling techniques, and five ESMs	Increase in AHV: +4.4 ± 7.4% Increase in AAV: +10.0 ± 16.5%
Temperature Changes		
<u>Irby et al., 2018</u>	Increased estuarine temperatures by 1.75 °C; assumed nutrient reductions	Increase in AHV: +13%
<u>Tian et al., 2021</u>	Increased atmosphere and ocean temperature increased by ~1 °C	†Increase in AHV: +9%
Sea Level Rise		
<u>Irby et al., 2018</u>	Increased sea level by 0.5 m; assumed nutrient reductions	Decrease in AHV: -13%
<u>St-Laurent et al., 2019</u>	Increased sea level by 0.5 m for 4 different models	Increase in summertime bottom O ₂ in all 4 models
<u>Cai et al., 2022</u>	Increased sea level by 0.5 m	Increase in AHV by +8%
<u>Cerco and Tian, 2022</u>	Increased sea level by 0.22 to 1 m and simulated wetland losses	Increase in DO criteria exceedances
Multiple Environmental Changes		
<u>Irby et al., 2018</u>	Combined atmosphere, watershed and sea level change, assuming nutrient reductions	Increase in AHV: +9%
<u>Ni et al., 2019**</u>	Combined atmosphere, watershed, and ocean Change: Multiple downscaled scenarios that increased air temperatures, monthly discharge, ocean temperatures and sea surface height	Increase in AHV: +9 to 31% Increase in AAV: +2 to 29%
<u>Basenback et al., 2022</u>	Modified timing of nutrient delivery and warming within the estuary	Change in AHV: -10% to +18%

AAV = Annual Anoxic Volume; AHV = Annual Hypoxic Volume

*AAV defined as O₂ < 1 mg L⁻¹ in Wang et al. (2017), and O₂ < 0.2 mg L⁻¹ for all others.

**Applied downscaled ESMs in projecting changes to Chesapeake Bay hypoxia.

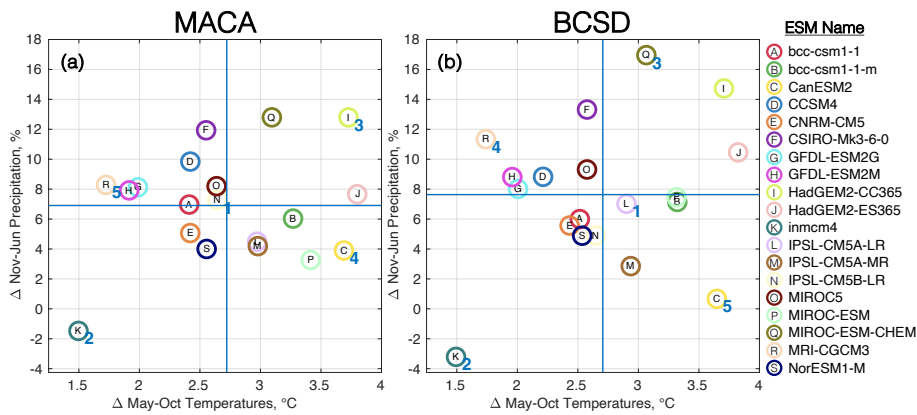
†No 2050 estimate provided; results based on 2025 projected changes.



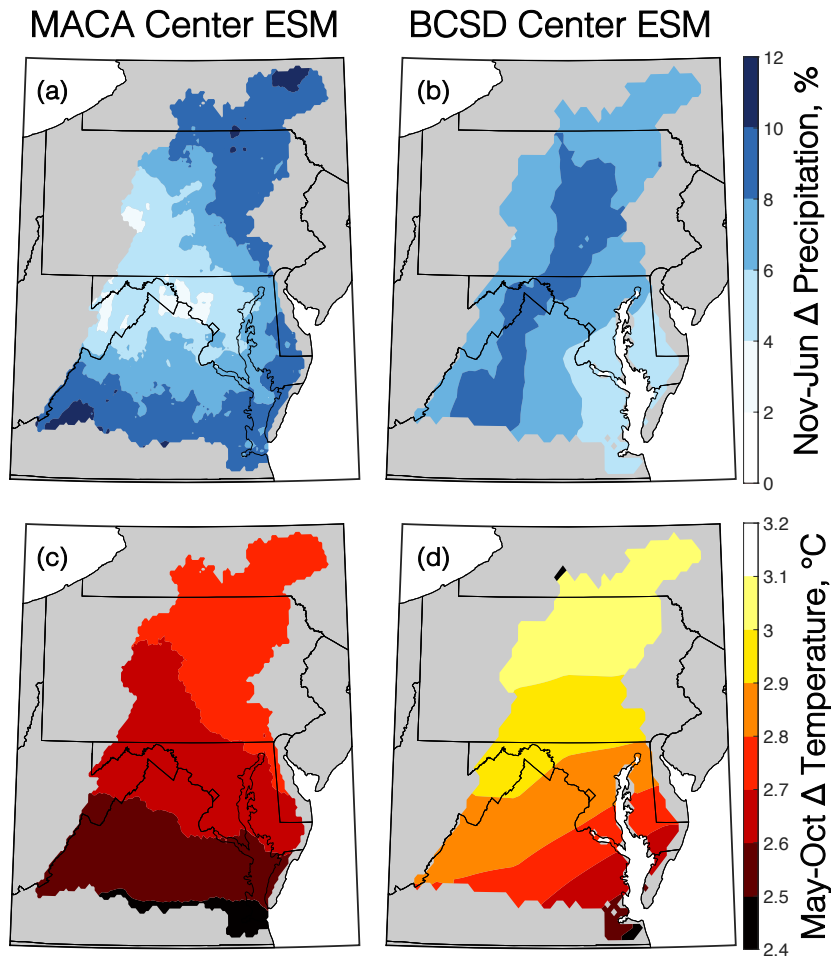
1471
 1472 **Figure 1:** (a) Map showing the extent of the Chesapeake Bay watershed boundary, major basins,
 1473 River Input Monitoring stations for the Susquehanna, Potomac, and James Rivers (red circles),
 1474 and ChesROMS-ECB river input locations (yellow circles). (b) Bathymetry of the ChesROMS-
 1475 ECB model domain, river input locations (yellow circles), and 20 Chesapeake Bay Program
 1476 main stem monitoring stations (green triangles).

Deleted: (RIM)

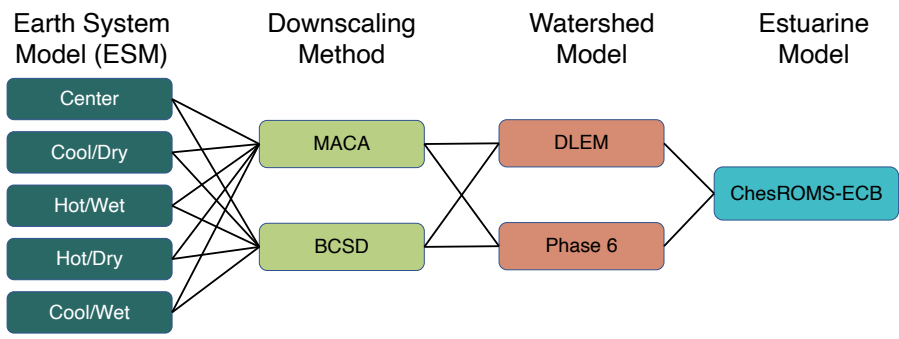
Deleted: CBP



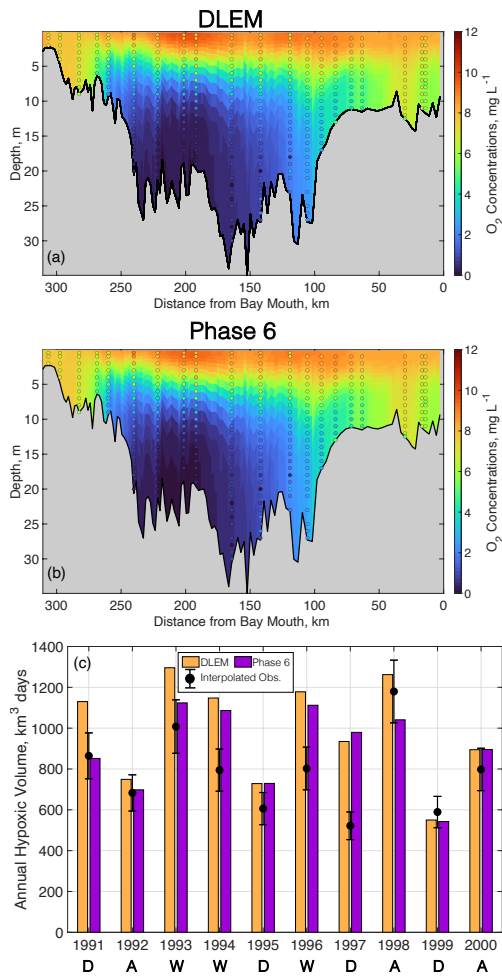
1479
 1480 **Figure 2:** Relative changes in May-October temperatures and November-June precipitation over
 1481 the Chesapeake Bay watershed for an ensemble of ESMs (circled letters) downscaled using (a)
 1482 MACA and (b) BCSD methodologies. Horizontal and vertical blue lines correspond to the
 1483 ensemble average changes in temperature and precipitation. Numbers adjacent to particular
 1484 ESMs in both panels denote the order in which the first five were selected by the KKZ algorithm.



1485
 1486 **Figure 3:** Changes in November to June precipitation (a, b) and May to October temperatures (c,
 1487 d) for the MACA (a, c) and BCSD (b, d) Center ESMs between mid-century (2046-2055) and the
 1488 reference period (1991-2000).

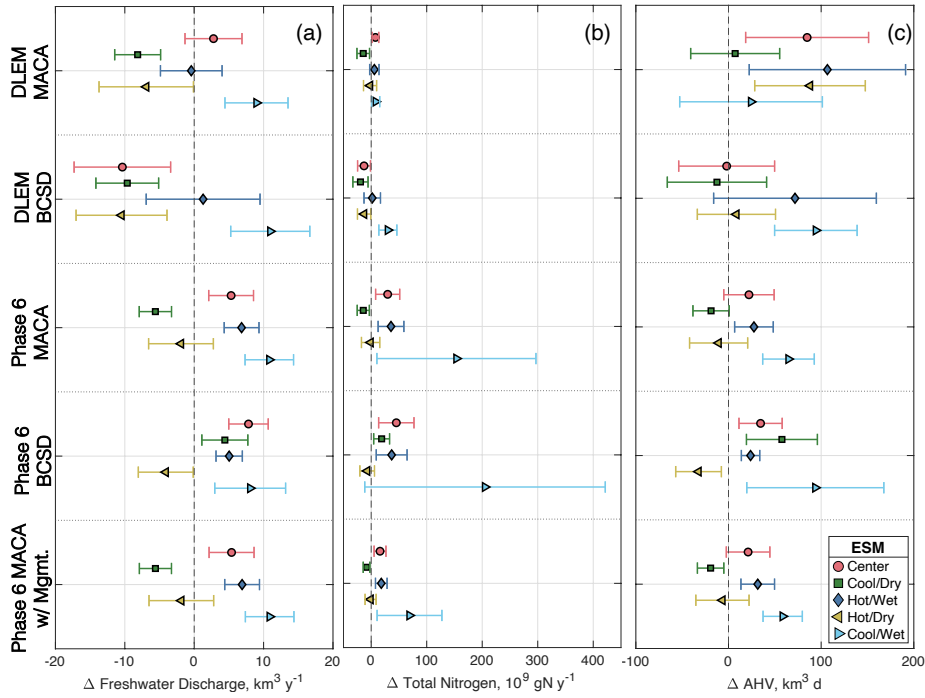


1489
 1490 **Figure 4:** Diagram of Multi-Factor experimental design, comprising a total of 20 model
 1491 scenarios.



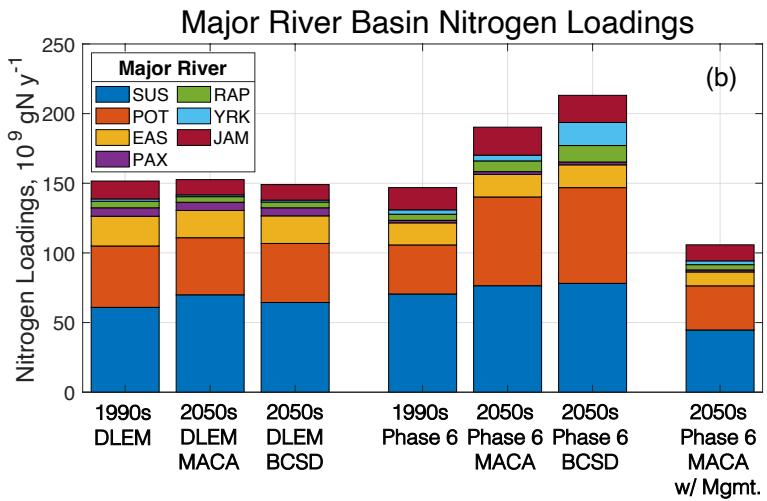
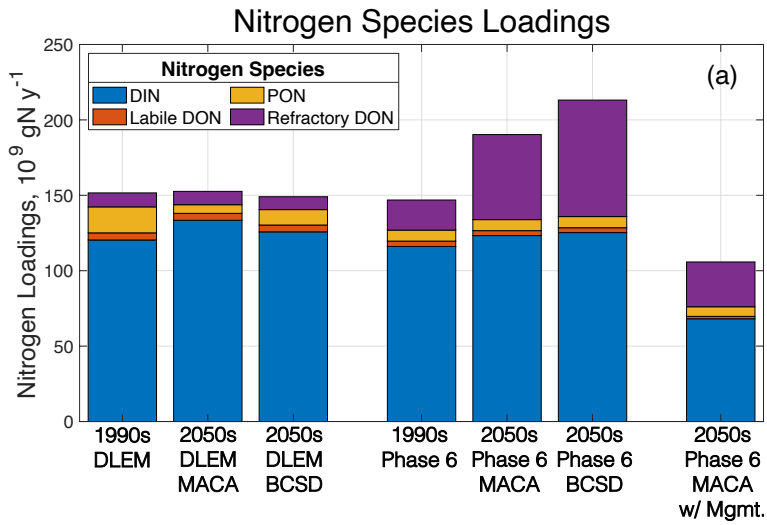
1492
 1493 **Figure 5:** ChesROMS-ECB skill for average summer (Jun-Aug) O₂ profiles at main stem
 1494 monitoring locations using watershed inputs from (a) DLEM and (b) Phase 6 over the reference
 1495 period 1991-2000. (c) Modeled AHV using DLEM and Phase 6 compared to interpolated
 1496 observations (error bars denote RMS percent error) over the reference period 1991-2000.
 1497 Average hydrologic conditions are noted below corresponding years and signify dry (D), average
 1498 (A), or wet (W) years.

1499



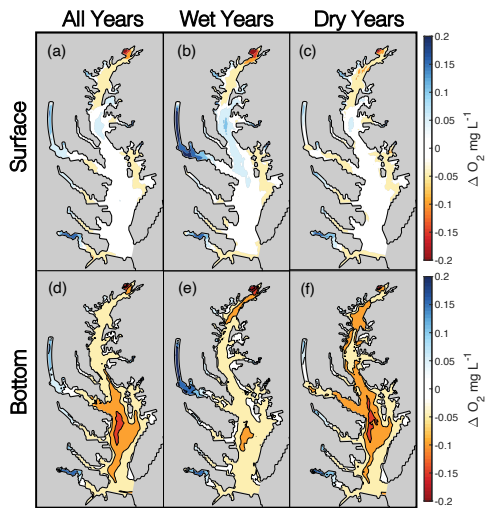
1500
1501
1502
1503
1504
1505
1506

Figure 6: Mean and standard deviations of changes to freshwater discharge (a), total nitrogen loadings (b), and annual hypoxic volume (c) for Multi-Factor and Management experiments. Future climate changes in these outputs are shown relative to 1990s baseline conditions (dashed vertical line) without management actions (upper four rows) and with management actions (bottom row).

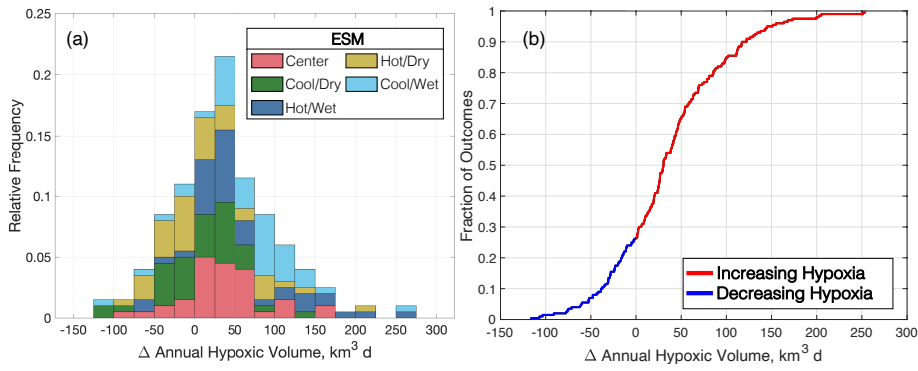


1507
 1508 **Figure 7:** Average total nitrogen loadings among ESM scenarios for reference scenarios and
 1509 various components of the Multi-Factor and Management experiments. Total nitrogen loadings
 1510 divided by (a) nitrogen species component: dissolved inorganic nitrogen (DIN), particulate
 1511 organic nitrogen (PON), dissolved organic nitrogen (DON), and refractory dissolved organic
 1512 nitrogen, and (b) by major river basin (SUS = Susquehanna, RAP = Rappahannock, POT =
 1513 Potomac, YRK = York, EAS denoting eastern shore rivers including the Elk, Chester, Choptank,
 1514 and Nanticoke, JAM = James, PAX = Patuxent).

Deleted: TN
 Deleted: TN



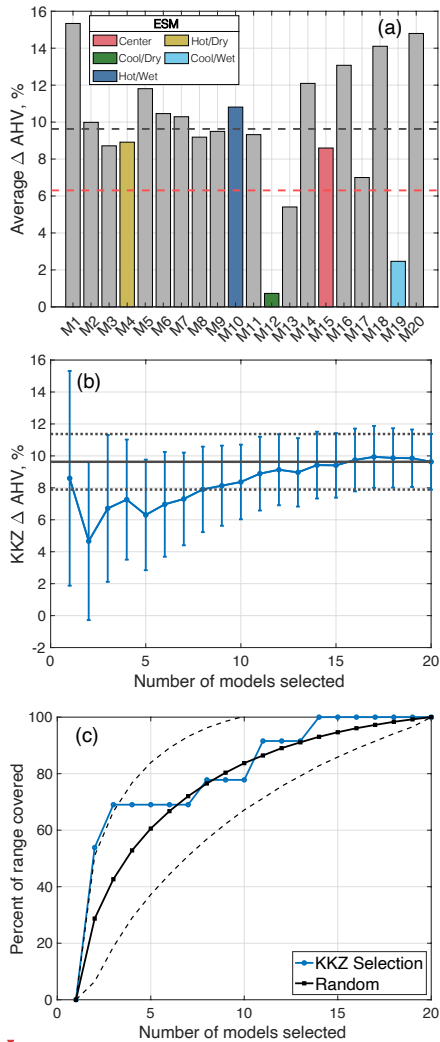
1517
 1518 **Figure 8:** Average O_2 changes in Multi-Factor experiment scenarios at the surface (a-c) and
 1519 bottom (d-f). Columns correspond to average changes for all years (a, d) as well as
 1520 hydrologically wet (b, e) and dry (c, f) years.



1521
1522
1523

Figure 9: Summary of Multi-Factor experiment results for changes to Annual Hypoxic Volume, expressed as a histogram of relative frequencies (a) and an empirical cumulative distribution (b).

Deleted: annual hypoxic volume



1525

1526

1527

1528

1529

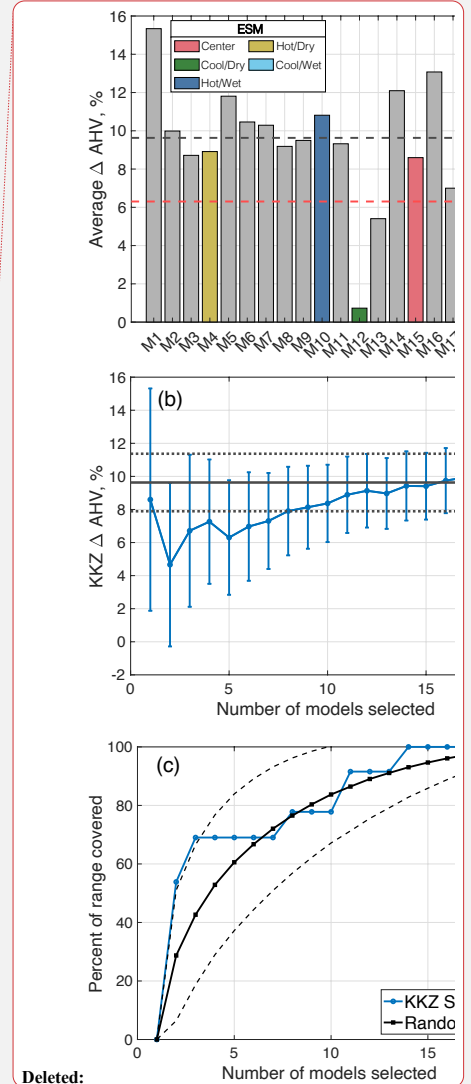
1530

1531

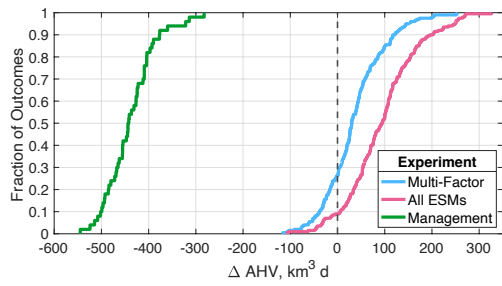
1532

1533

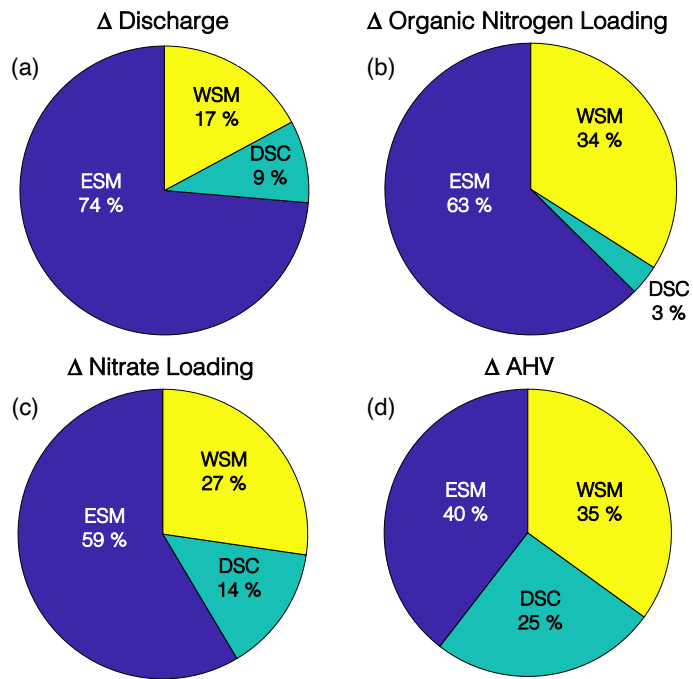
Figure 10: (a) **Change in Annual Hypoxic Volume (Δ AHV)** for the All-ESMs experiment. Red dashed line denotes the multi-model average of five KKZ-selected ESMs; black dashed line denotes the full 20-model average. (b) Δ AHV and standard errors as estimated by increasing number of KKZ-selected ESMs. Black lines correspond to 20-model average (solid) and associated standard errors (dotted) from the All-ESMs experiment. (c) Percent of Δ AHV range covered by sequentially increasing the number of KKZ-selected ESMs. Black lines correspond to the range (solid) and associated standard error (dashed) of estimates chosen by randomly selecting ESMs.



Deleted:



1535
 1536 **Figure 11:** Summary of all experiment results for change in Annual Hypoxic Volume (Δ AHV),
 1537 expressed as a cumulative distribution function. Black dashed vertical line corresponds to no
 1538 change in AHV.



1539
 1540 **Figure 12:** Percent contribution to uncertainty from Earth System Model (ESM), downscaling
 1541 methodology (DSC), and watershed model (WSM), for estimates of (a) discharge, (b) organic
 1542 nitrogen loading, (c) nitrate loading, and (d) change in annual hypoxic volume (Δ AHV).

Page 12: [1] Deleted Kyle Hinson 3/30/23 8:32:00 PM

Page 12: [2] Deleted Kyle Hinson 3/30/23 8:32:00 PM

Page 12: [3] Deleted Kyle Hinson 3/30/23 8:32:00 PM